Structural analysis reveals features of the spindle checkpoint kinase Bub1–kinetochore subunit Knl1 interaction

Veronica Krenn,[1] Annemarie Wehenkel,[1,2] Xiaozheng Li,[1] Stefano Santaguida,[1] and Andrea Musacchio[1,2]

[1]Department of Experimental Oncology, European Institute of Oncology, 20139 Milan, Italy
[2]Department of Mechanistic Cell Biology, Max Planck Institute of Molecular Physiology, 44227 Dortmund, Germany

The function of the essential checkpoint kinases Bub1 and BubR1 requires their recruitment to mitotic kinetochores. Kinetochore recruitment of Bub1 and BubR1 is proposed to rely on the interaction of the tetratricopeptide repeats (TPRs) of Bub1 and BubR1 with two KI motifs in the outer kinetochore protein Knl1. We determined the crystal structure of the Bub1 TPRs in complex with the cognate Knl1 KI motif and compared it with the structure of the equivalent BubR1TPR–KI motif complex. The interaction developed along the convex surface of the TPR assembly. Point mutations on this surface impaired the interaction of Bub1 and BubR1 with Knl1 in vitro and in vivo but did not cause significant displacement of Bub1 and BubR1 from kinetochores. Conversely, a 62-residue segment of Bub1 that includes a binding domain for the checkpoint protein Bub3 and is C terminal to the TPRs was necessary and largely sufficient for kinetochore recruitment of Bub1. These results shed light on the determinants of kinetochore recruitment of Bub1.

Introduction

The spindle assembly checkpoint, or mitotic checkpoint, coordinates mitotic timing with chromosome–spindle interactions during mitosis, restricting mitotic exit to cells that have achieved biorientation of all their chromosomes (Musacchio and Salmon, 2007). Cells in which the checkpoint is artificially inactivated undergo precocious mitotic exit in the presence of unattached or incorrectly attached chromosomes. Alterations of checkpoint function might be relevant for tumor development, possibly by rendering cells more susceptible to the development of aneuploidies and to consequent genetic instability (Kolodner et al., 2011).

Bub1 (budding uninhibited by benzimidazole 1) was originally characterized as a conserved component of the spindle assembly checkpoint (Hoyt et al., 1991; Taylor and McKeon, 1997; Musacchio and Salmon, 2007). More recently, Bub1 was also shown to play a function in chromosome alignment (Johnson et al., 2004; Meraldi and Sorger, 2005; Windecker et al., 2009). Precisely how Bub1 performs these functions at the molecular level is unclear (Bolanos-Garcia and Blundell, 2011; Elowe, 2011). Bub1 localization at kinetochores, in which it displays slow exchange dynamics during mitosis (Howell et al., 2004; Shah et al., 2004), might be important or even essential for its functions. Bub1 phosphorylates Cdc20, the target of the checkpoint, on several sites, promoting its ability to engage in an inhibitory complex with other checkpoint proteins (Tang et al., 2004a). Moreover, Bub1 promotes kinetochore recruitment of other checkpoint proteins, including Mad1, Mad2, Mad3/BubR1 (Bub1 related), and Bub3. Such recruitment is in turn believed to be important for the activity of these proteins (Sharp-Baker and Chen, 2001; Chen, 2002; Johnson et al., 2004; Vigneron et al., 2004; Meraldi and Sorger, 2005; Boyarchuk et al., 2007; Rischitor et al., 2007; Klebig et al., 2009; Storchová et al., 2011). Bub1 also phosphorylates H2A (histone 2A), promoting the recruitment of Sgo1 and Aurora B to the centromere (Kitajima et al., 2004, 2005; Tang et al., 2004b; Vaur et al., 2005; Fernius and Hardwick, 2007; Perera et al., 2007; Yamagishi et al., 2010; Kawashima et al., 2010; Wang et al., 2011).

V. Krenn, A. Wehenkel, and X. Li contributed equally to this paper.

Correspondence to Andrea Musacchio: andrea.musacchio@mpi-dortmund.mpg.de

S. Santaguida's present address is David H. Koch Institute for Integrative Cancer Research, Massachusetts Institute of Technology, Cambridge, MA 02139.

Abbreviations used in this paper: GLEBS, Gle2 binding site; IRES, internal ribosomal entry site; TPR, tetratricopeptide repeat.

The Rockefeller University Press $30.00
J. Cell Biol. Vol. 196 No. 4 451–467
www.jcb.org/cgi/doi/10.1083/jcb.201110013

BubR1, whose overall domain organization is very similar to that of Bub1 (Fig. 1 A), is also implicated both in the spindle checkpoint and in chromosome alignment (Li and Murray, 1991; Taylor et al., 1998; Chan et al., 1999; Johnson et al., 2004; Lampson and Kapoor, 2005). Unlike Bub1, BubR1 is incorporated together with Bub3, Mad2, and Cdc20 in the checkpoint effector, the so-called mitotic checkpoint complex, which inactivates the anaphase-promoting complex/cyclosome to prevent mitotic exit (Musacchio and Salmon, 2007).

Kinetochore recruitment of Bub1 and BubR1 may be strongly intertwined with their activation and functions there. For instance, kinetochore localization of Bub1 and BubR1 might be important for their phosphorylation, which in turn contributes to the functions of these kinases (Yamaguchi et al., 2003; Elowe et al., 2010). The exact mechanism of kinetochore recruitment of Bub1 and BubR1, however, remains unclear. It was originally shown that ∼300 residues in the N-terminal region of murine Bub1 (shown schematically in Fig. 1 A) are sufficient for kinetochore localization (Taylor and McKeon, 1997; Taylor et al., 1998). This region of Bub1 includes an array of three tetratricopeptide repeats (TPRs; D'Arcy et al., 2010; Bolanos-Garcia et al., 2011, 2009) followed by a motif, also present in BubR1, which binds to the checkpoint protein Bub3 (Taylor et al., 1998). Bub3 is a β-propeller structure that uses its top surface to interact directly with the Bub3-binding motifs of Bub1 and BubR1/Mad3 (Larsen et al., 2007). The Bub3-binding motif is now also often referred to as the Gle2 binding site (GLEBS) motif (Wang et al., 2001). Here, however, we prefer to use the name Bub3-binding domain (abbreviated as Bub3-BD) because there is no evidence, to our knowledge, that Bub1 and BubR1 interact with the Gle2 protein (also known as Rae1).

Further deletion mapping of Bub1 demonstrated that the TPR region is dispensable for kinetochore localization and that a segment containing the Bub3-BD might be sufficient for kinetochore localization (Taylor et al., 1998). Mutations in the Bub3-BD prevent kinetochore localization of Bub1 and BubR1 and impair BubR1's function in checkpoint and chromosome congression (Taylor et al., 1998; Klebig et al., 2009; Malureanu et al., 2009; Elowe et al., 2010). As the only known function of the Bub3-BD of Bub1 and BubR1 is Bub3 binding, these data argue that the interaction of Bub1 and BubR1 with Bub3 might be necessary and sufficient for their kinetochore localization. Partly contradicting this idea, however, depletion of Bub3 does not affect Bub1 localization, whereas it might affect the localization of BubR1 (Meraldi et al., 2004; Logarinho et al., 2008). Conversely, depletion of Bub1 or BubR1 was found to reduce kinetochore recruitment of Bub3, suggesting that these proteins are not simply recruited by Bub3 (Sharp-Baker and Chen, 2001; Chen, 2002).

More recently, insight into the mechanism of kinetochore recruitment of Bub1 and BubR1 developed around the discovery that their TPRs interact with the outer kinetochore protein Knl1 (also known as Blinkin, CASC5, and AF15q14 in human cells, Spc105 in *Saccharomyces cerevisiae*, and Spc7 in *Schizosaccharomyces pombe*; Kiyomitsu et al., 2007, 2011; Schittenhelm et al., 2009). Knl1 is a subunit of the KMN network, a 10-subunit assembly of three complexes, the Knl1 complex (KNL1-C, comprised of Knl1 and Zwint-1), the MIS12 complex (MIS12-C, comprised of Mis12/Mtw1, Dsn1, Nnf1, and Nsl1), and the NDC80 complex (NDC80-C, comprised of Ndc80/Hec1, Nuf2, Spc24, and Spc25). The KMN network mediates microtubule attachment through microtubule-binding domains located in the Ndc80 and Knl1 subunits (Cheeseman and Desai, 2008; Santaguida and Musacchio, 2009). It has also been implicated in the recruitment of all known checkpoint proteins, suggesting that it plays a crucial role in relaying microtubule attachment status to the spindle checkpoint response.

The TPRs of Bub1 and BubR1 interact with distinct, but related, 12-residue motifs in the N-terminal region of Knl1, the KI motifs (from the first two residues of their consensus sequence, KI(D/N)XXXF(L/I)XXLK, in which X's are nonconserved residues; Fig. 1 A; Bolanos-Garcia et al., 2011; Kiyomitsu et al., 2011). The two consecutive motifs are herewith indicated as KI1 and KI2. Although it was originally hypothesized that these interactions might engage residues on the concave surface of the superhelically twisted TPR repeat assemblies of Bub1 and BubR1 (D'Arcy et al., 2010; Kiyomitsu et al., 2011), a very recent structural analysis of the BubR1–KI2 complex revealed that the KI2 motif of Knl1 engages the convex surface of the BubR1 TPR region (Bolanos-Garcia et al., 2011).

The potential importance of the interaction of the KI motif of Knl1 with the Bub1 TPRs is underpinned by the observation that a point mutant in the TPRs prevents kinetochore recruitment of Bub1 (Kiyomitsu et al., 2007). Furthermore, depletion of Knl1 by RNAi prevents kinetochore recruitment of Bub1 and BubR1 (Kiyomitsu et al., 2007). Finally, a deletion mutant lacking the TPRs of Bub1 failed to localize to kinetochores, reinvigorating the previously dismissed idea that this region of Bub1 participates in kinetochore recruitment (Klebig et al., 2009). Thus, both the N-terminal TPRs and the Bub3-BD, which bind to Knl1 and Bub3, are thought to contribute to kinetochore recruitment of Bub1 and BubR1, but there is no unifying view of the relative importance of their contributions. We have therefore set out to clarify this important question.

Results

Role of the TPRs of Bub1 and BubR1 in kinetochore recruitment

We tested whether the TPR domain of human Bub1 (included in two constructs encompassing residues 1–150 or residues 1–190) is sufficient for kinetochore binding in HeLa cells. Expression of EGFP fusions of wild-type full-length Bub1 (Bub1(FL)) resulted in bright kinetochore staining (Fig. 1 B and Fig. S1 for expression levels of the transgenes). On the other hand, EGFP fusions of Bub1(1–150) or Bub1(1–190) failed to localize to kinetochores (Fig. 1 B). These results suggest that the TPR region of Bub1 is not sufficient for kinetochore localization. We next tested whether this region is necessary for kinetochore binding. Bub1 mutants lacking either 150 or 189 residues from their N terminus (Bub1(Δ150) or Bub1(Δ189)) localized normally to kinetochores (Fig. 1 B). It is unlikely that these results were

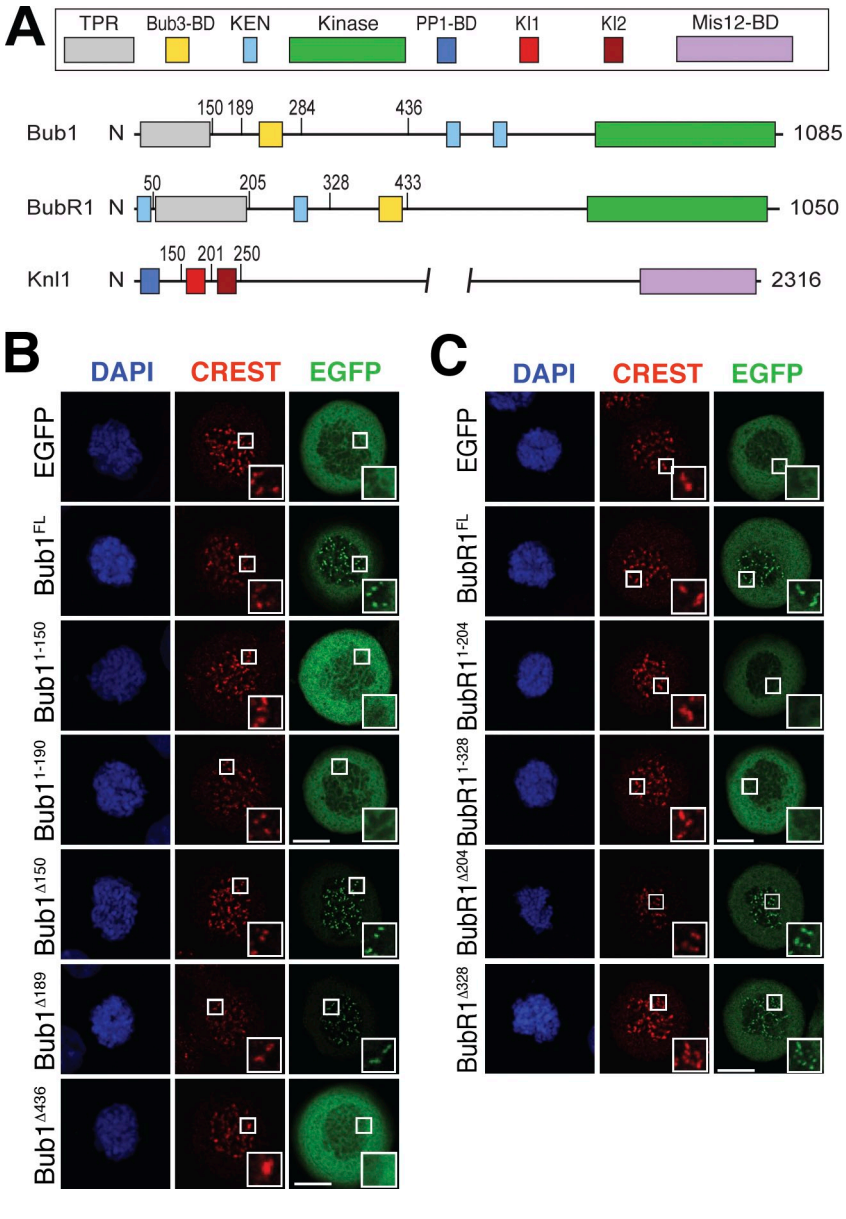

Figure 1. **TPRs are not sufficient or necessary for kinetochore recruitment of Bub1 and BubR1.** (A) Schematic view of the domain structure of Bub1, BubR1, and Knl1; TPR, tetratricopeptide repeats; Bub3-BD, Bub3-binding domain, also known as GLEBS motif; KEN, KEN box; PP1-BD, protein phosphatase 1–binding domain; KI1, Bub1-binding domain 1; KI2, BubR1-binding domain 2; Mis12-BD, Mis12-binding domain; N, N terminus. (B and C) Immunofluorescence images of mitotic cells expressing different Bub1 (B) and BubR1 (C) constructs. HeLa cells were transiently transfected with plasmids containing EGFP alone, N-terminally EGFP-tagged Bub1, or BubR1 constructs. Cells were treated with nocodazole, processed for immunofluorescence, and stained with DAPI (DNA) and CREST (calcinosis, Raynaud's phenomenon, esophageal dysmotility, sclerodactyly, and telangiectasia) sera (kinetochores). Insets show a higher magnification of kinetochore regions (boxes). Bars, 5 µm. All images were acquired within the same experiment.

an artifact from fusing EGFP at the N terminus of the Bub1 deletion constructs because a C-terminal fusion of Bub1(Δ189) also localized normally to kinetochores (Fig. S1, E and F). When we created longer deletions and removed the first 436 residues (Bub1(Δ436)), the resulting Bub1 construct failed to localize to kinetochores (Fig. 1 B). These results suggest that residues 190–436, from which the TPR repeats of Bub1 are excluded, might be necessary for kinetochore recruitment of Bub1.

We next tested whether the TPR domain of BubR1 is important for kinetochore recruitment. Two constructs encompassing residues 1–204 and 1–328, which include the TPR region (Fig. 1 A), were expressed in HeLa cells and found to be unable to reach kinetochores (Fig. 1 C and Fig. S1 C for expression levels of the transgenes). Analogously to the results obtained with Bub1 deletion mutants, deletion of the TPR domain of BubR1 (BubR1(Δ204) or BubR1(Δ328)) did not evidently affect kinetochore recruitment (Fig. 1 C and Fig. S1 D). Overall, these results indicate that the TPR region of Bub1 and BubR1 is neither sufficient, nor strictly necessary, for kinetochore recruitment.

The TPR domains of Bub1 and BubR1 bind Knl1 directly

The TPR regions of Bub1 and BubR1 have been previously shown to mediate an interaction with the kinetochore protein Knl1 and have been suggested to promote the recruitment of Bub1 and BubR1 to kinetochores via this interaction (Kiyomitsu et al., 2007, 2011; Klebig et al., 2009; D'Arcy et al., 2010). Our results in Fig. 1, however, indicate that the TPR region of Bub1 is neither sufficient nor necessary for kinetochore recruitment. To reconcile these apparently contradictory observations, we hypothesized a more complex recruitment model. We speculated that an intramolecular interaction involving the N-terminal TPR motif might be masking a high-affinity,

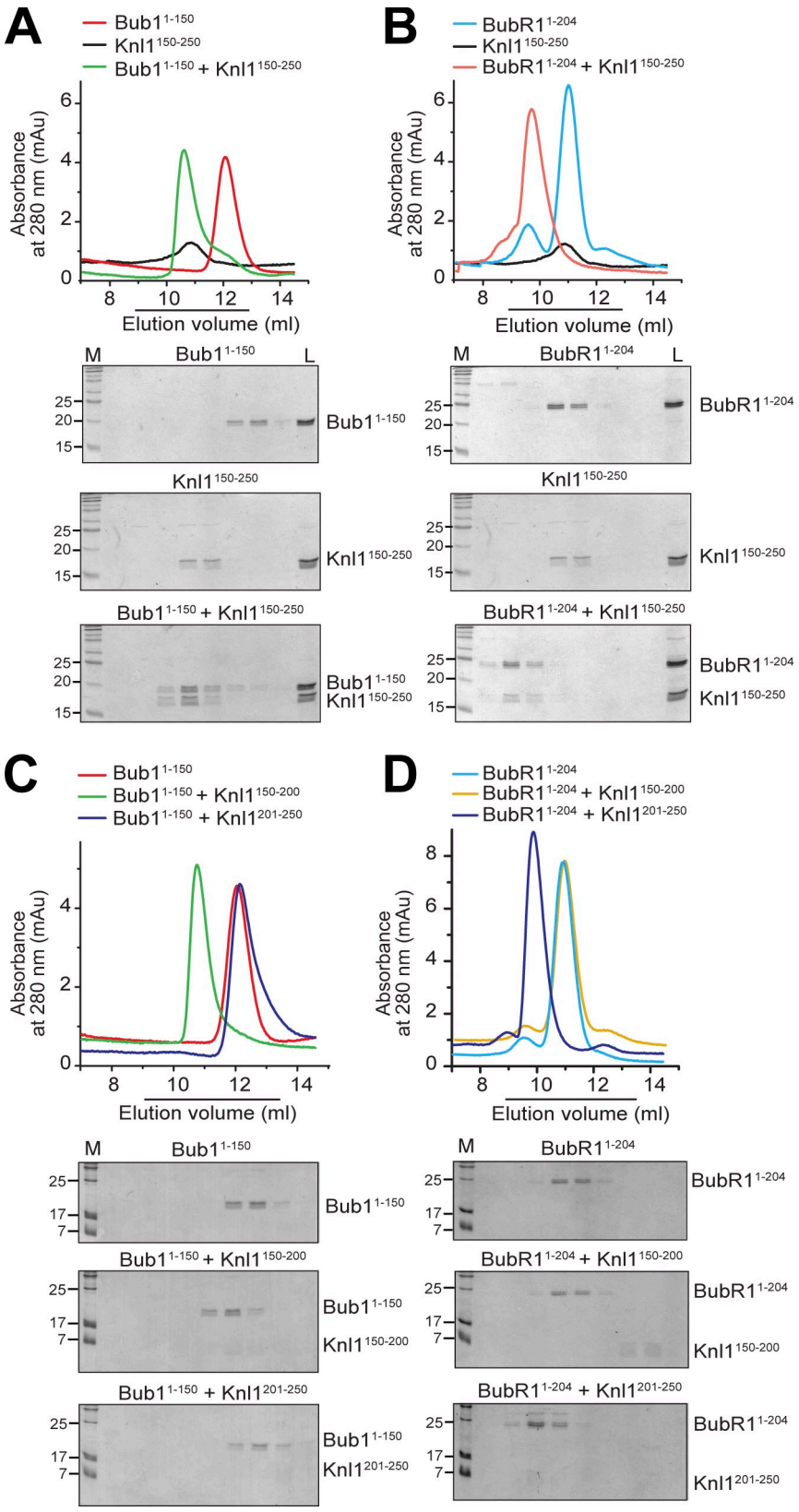

Figure 2. **Direct binding of Bub1 and BubR1 TPRs to Knl1 KI motifs.** (A) The interaction of Bub1(1–150) with Knl1(150–250) was analyzed by size-exclusion chromatography, which separates based on size and shape. (B) Analysis of the interaction of BubR1(1–204) with Knl1(150–250). (C) Analysis of the interaction of Bub1(1–150) with Knl1(150–200) or Knl1(201–250). (D) Analysis of the interaction of BubR1(1–204) with Knl1(150–200) or Knl1(201–250). M, molecular mass marker; L, sample loaded on the column. The same elution profile for Knl1(150–250) was used as a control for A and B. Molecular markers are given in kilodaltons. mAu, milliabsorbance unit.

secondary kinetochore-binding domain in Bub1 and BubR1. This secondary site would provide the bulk of the kinetochore-binding affinity but should only become exposed after the initial binding of Knl1 to the TPR motifs. In such a model, deletion of the TPR region is predicted not only to remove the Knl1 binding site but also to relieve an intramolecular inhibitory function, with the consequent constitutive exposure of the high-affinity binding site even in the absence of Knl1 binding.

An implication of the model is that if one were able to selectively perturb the interaction of Bub1 with Knl1, without disrupting the hypothetical intramolecular switch, the resulting mutant impaired in Knl1 binding might also be impaired in kinetochore binding as a consequence of constitutive inhibition. Testing this model required a better understanding of the structural basis of the interaction of the Bub1 and BubR1 TPRs with Knl1, so as to allow the creation of separation of function mutants. Thus, we attempted to unveil the biochemical and structural basis of this interaction. Because it is formally undemonstrated that the interaction of Bub1 and BubR1 with Knl1 is direct, we expressed and purified recombinant versions of Bub1(1–150) and BubR1(1–204) and tested their ability to bind to Knl1 constructs encompassing the previously identified KI motifs (depicted in Fig. 1 A; Kiyomitsu et al., 2011). When analyzed by size-exclusion chromatography (a technique that allows the separation of macromolecules based on their size and shape), Bub1(1–150) and BubR1(1–204) were shown to form stoichiometric complexes with Knl1(150–250), a construct that encompasses both the KI1 and the KI2 motif (Fig. 2, A and B). Conversely, Bub1(1–150) bound to Knl1(150–200), which contains the KI1 motif (Fig. 2 C), but was unable to bind to Knl1 (201–250), which contains the KI2 motif. Precisely the opposite result was obtained with BubR1(1–204). The latter bound Knl1 (201–250), which contains the KI2 motif, but not Knl1(150–200), which contains the KI1 motif (Fig. 2 D). Thus, the TPR motifs of Bub1 and BubR1 bind directly and specifically to the KI1 and KI2 motif, respectively.

Crystal structure of the Bub1(1–150)–Knl1(150–200) complex

Next, we determined the crystal structure of the Bub1(1–150)–Knl1(150–200) complex. Single crystals of the complex diffracted to a maximal resolution of 2.6 Å in the space group $P2_1$ (Table 1). The four Bub1(1–150)–Knl1(150–200) complexes in the asymmetric unit are very similar, with the only exceptions occurring at intersubunit contacts. The description that follows refers to the general features of the complexes.

TPR repeats form helical hairpins, i.e., arrangements of two antiparallel α helices, denoted A and B. Subsequent repeats pack against each other, usually forming arrays of 3–16 repeats that are characterized by a right-handed superhelical twist that generates concave and convex surfaces. There are three TPR repeats in Bub1(1–150) (comprising helices α2–α7), capped by N-terminal and C-terminal helices (α1 and α8, respectively; Fig. 3 A). TPRs or equivalent arrangements of helical hairpins, such as HEAT repeats, usually bind their substrates on the concave surface, a cradle for elongated protein ligands. In the case of Bub1(1–150)–Knl1(150–200), however, the Knl1 sequence binds to a moderately conserved ridge on the convex surface of Bub1 (Fig. 3, A and B). Secondary structure and level of conservation are depicted in Fig. 3 C. On the concave surface, there is a distinct ridge that might provide a binding site for another substrate or for an intramolecular interaction.

There is interpretable electron density for residues 175–189 of Knl1, whereas the rest of the polypeptide chain is presumably disordered in solvent and therefore invisible in the electron density. Thus, the structure is in agreement with the idea that the Bub1 binding site on Knl1 is essentially limited to the previously identified KI motif (Kiyomitsu et al., 2011). The dissociation constant (K_d) for the interaction of Bub1(1–150) with a fluorescent synthetic peptide corresponding to Knl1 residues 174–190, measured by fluorescence polarization anisotropy, was ∼35 µM (Fig. 4 B). In the structure, most of the KI motif folds as a short α helix that lies on the convex surface of Bub1. Several Knl1 residues, including Ile177, Thr179, and Phe182, point toward the Bub1 surface. These residues make extensive van der Waals contacts with the Bub1 surface (Fig. 4 A). Additionally, there are hydrogen bonds between Thr179(Knl1) and Thr180(Knl1) with Gln84(Bub1). These observations are consistent with a previous analysis of the effects of mutations in the KI1 motif of Knl1 on Bub1 binding (Kiyomitsu et al., 2011). On Bub1, the A-type helix α4 contributes the side chains of Phe75 and Asn79, thus participating from the bottom to the creation of the Knl1-binding ridge. The B-type α3 and α5 helices surround the ridge, with α5 contributing the side chains of Gln84, Phe85, and Phe88 (Fig. 4 A).

Table 1. **Data collection used in this paper**

Variable	Value
Beamline	ESRF ID14 EH1
a (Å)	59.3
b (Å)	131
c (Å)	75
α and γ (°)	90
β (°)	110.2
Space group	$P2_1$
Wavelength (Å)	0.9334
Resolution	65-2.6 (2.74-2.60)
Completeness (%)	98.8 (99.6)
Multiplicity	2.8 (2.8)
Mean (I)/σ(I)	13.7 (3.2)
R_{meas}	0.072 (0.50)

Numbers in parentheses correspond to the highest resolution shell. R_{meas} is the multiplicity-weighted merging R factor according to Diederichs and Karplus (1997). I, reflection intensity.

In vitro and in vivo validation of the Bub1–Knl1 interaction

We individually mutated Phe75, Asn79, Gln84, and Phe85 to alanine and evaluated the ability of the mutants to bind Knl1(150–250) by size-exclusion chromatography (mutation of Phe88 to alanine rendered the protein insoluble when expressed in *Escherichia coli*; Fig. 4 C). We observed essentially complete disruption of the Bub1(1–150)–Knl1(150–250) complex in three out of four cases (only the Gln84 to Ala mutant had mild or no effects on binding). The results confirm the role of the interface on the convex surface of Bub1 in Knl1 binding in vitro.

Next, we tested the effects of Bub1 mutations on the ability of Bub1 to bind Knl1 in vivo. For this, we generated stable inducible cell lines expressing EGFP-tagged wild-type Bub1 and a mutant carrying the four alanine mutations characterized in Fig. 4 C (Bub1(4A)). We next evaluated the interaction of

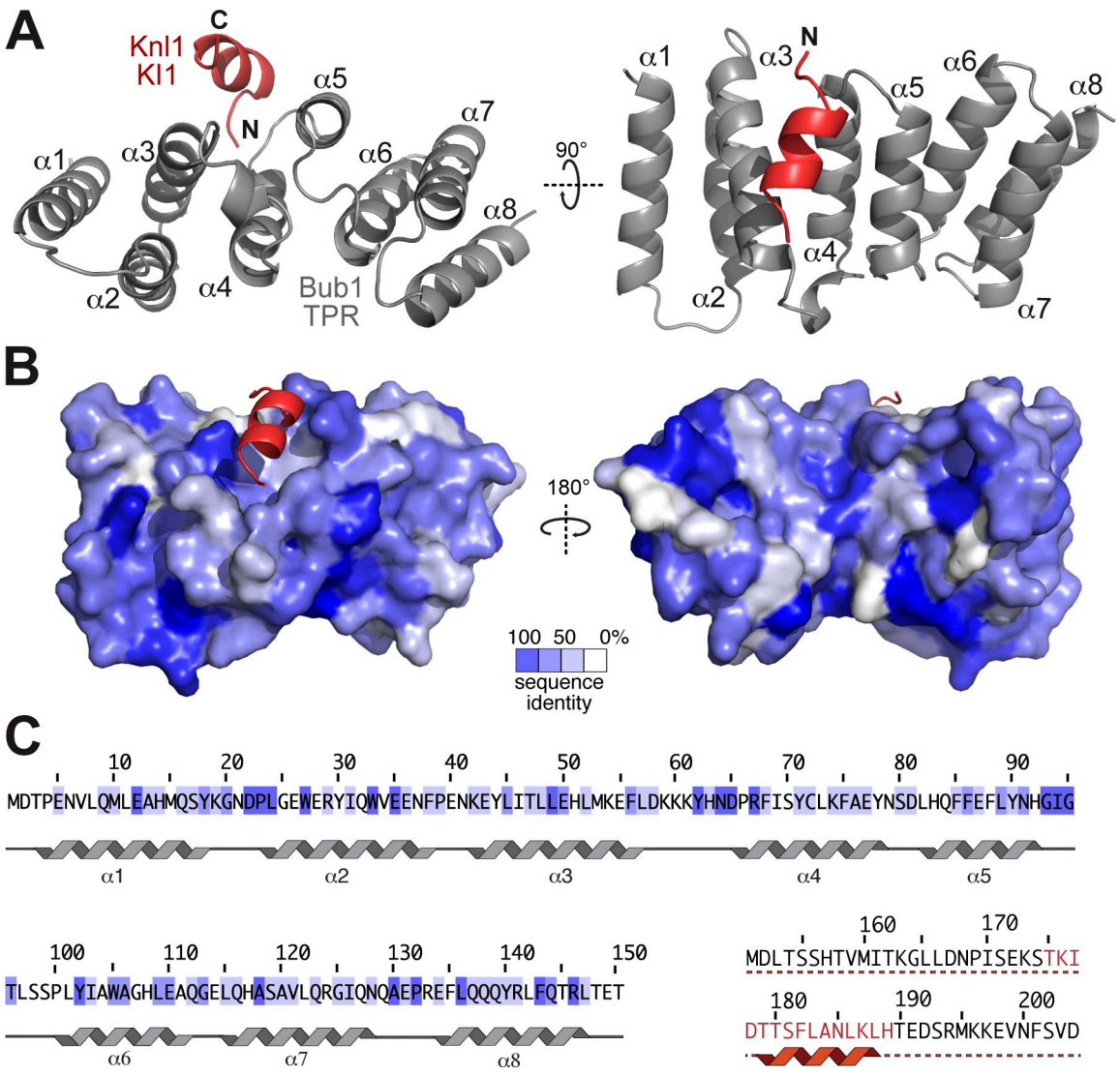

Figure 3. **Crystal structure of the Bub1(1–150)–Knl1(150–200) complex.** (A) Side and top view of a cartoon representation of Bub1(1–150) (gray) and Knl1 peptide (red). (B) Surface representation of the complex, oriented so as to show the convex (left) and concave (right) side. Sequence conservation (limited to Bub1 orthologues) was mapped onto the Bub1 structure using ConSurf (Ashkenazy et al., 2010). The structure was illustrated using PyMOL (Delano Scientific, LLC). (C) Sequence of the Bub1 (gray) and Knl1 (red) fragments used for crystallization. Secondary structure elements are mapped onto the sequence. C, C terminus; N, N terminus.

these constructs with endogenous Knl1, Hec1, and Mis12 by GFP immunoprecipitation followed by Western blotting. The Bub1(4A) mutant was severely impaired in its ability to interact with Knl1, and only modest residual binding was retained (Fig. 4 D). Because Knl1 interacts directly with other components of the KMN network, including subunits of the Mis12 and Ndc80 complexes (Cheeseman et al., 2006; Petrovic et al., 2010), the levels of Mis12 and Ndc80 were also reduced. Analogous results were obtained with the Bub1(Δ189) deletion mutant (Fig. 4 D). These results strongly support the view, based on the crystal structure, that the convex surface of the Bub1 TPR region contributes to Knl1 binding in cells.

Interaction of BubR1 with Knl1

The sequences of the TPR regions of Bub1 and BubR1 are closely related (Fig. 5 A). Similarly, the sequences of the previously identified KI motifs of Knl1 are also closely related (Fig. 5 B). By fluorescence polarization anisotropy, we determined that the binding affinity of BubR1(1–204) for a synthetic fluorescent peptide corresponding to Knl1(210–226) is 0.45 µM, almost 100-fold tighter than the value measured for the interaction of Bub1(1–150) to Knl1(174–190) (Fig. 4 B and Fig. 5 C). The significance of this difference in binding affinity is currently unclear but might be caused by a technical limitation of the assay, as we note that Bub1(1–150) interacts stoichiometrically with Knl1(150–250) or Knl1 (150–200) when the individual proteins are mixed at a concentration of 5 µM, suggesting that the K_d of the interaction may realistically be lower (i.e., higher affinity. See Materials and methods for details on the assay).

While this paper was under review, the crystal structure of the complex of human BubR1 TPR region bound to the KI2 motif was published (Protein Data Bank accession no. 3SI5; Bolanos-Garcia et al., 2011). The BubR1 backbone superimposes on the Bub1 TPR structure with a root-mean-square

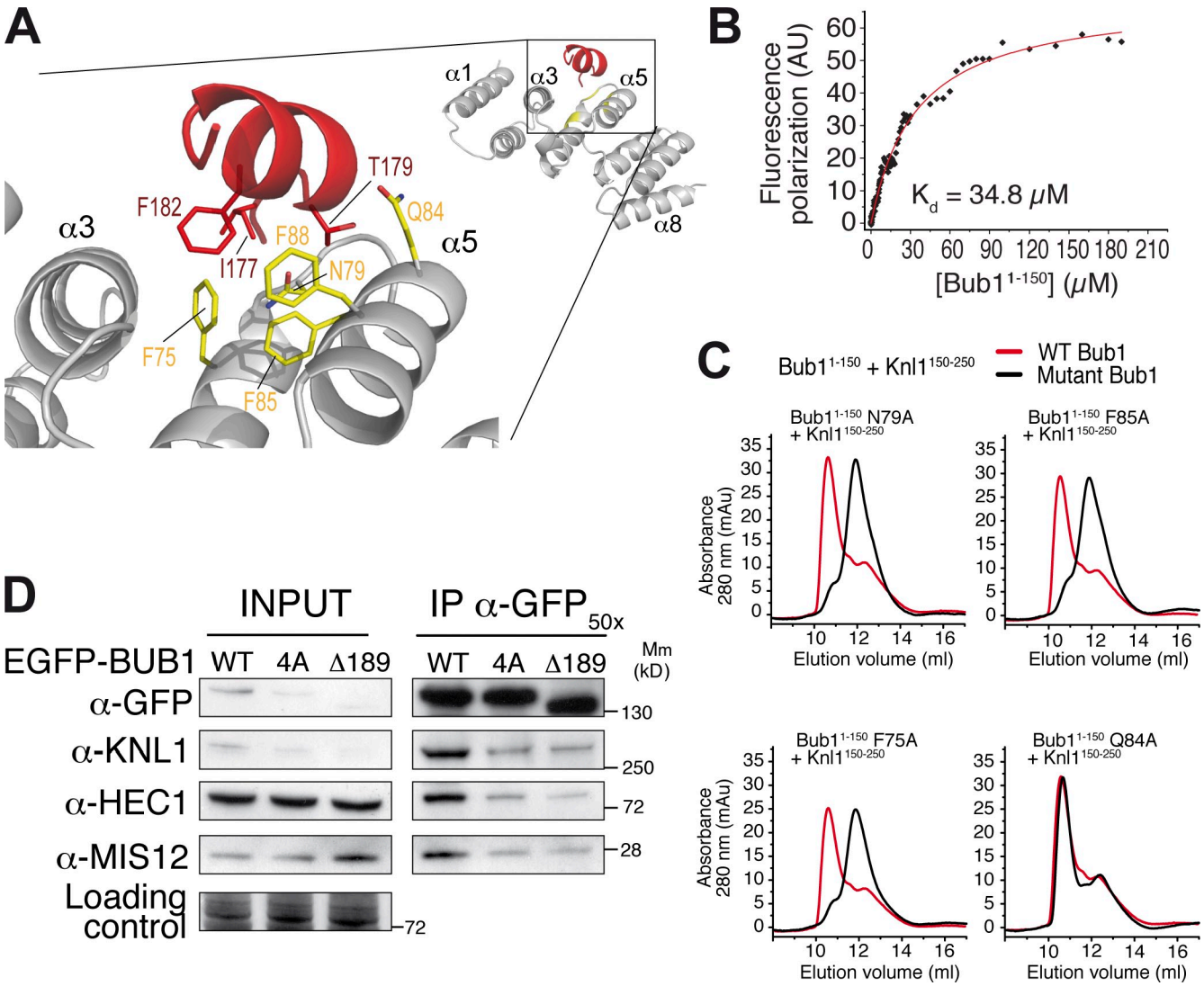

Figure 4. **Validation of the Bub1(1–150)–Knl1(150–200) binding mechanism.** (A) Close-up of the interaction of the Knl1–Bub1 interaction (red and gray, respectively). (B) Fluorescence polarization anisotropy experiments for the interaction of a fluorescent version of Knl1(174–190) with Bub1(1–150). Red line is a fit of the data with the equation discussed in Materials and methods, Fluorescence anisotropy. AU, absorbance units. (C) Elution profiles for size-exclusion chromatography runs for binding reactions of the indicated Bub1(1–150) mutants with Knl1(150–250). The elution profile for the interaction of wild-type Bub1(1–150) with Knl1(150–250) is shown in red. The same control profile is shown in all graphs, with its height scaled to the height of the profile of mutant. (D) Immunoprecipitation of EGFP-tagged Bub1(WT), Bub1(4A), and Bub1(Δ189). Bub1(4A) contains the F75A, N79A, Q84A, and F85A mutations. Mitotic extracts from stable inducible cell lines expressing various EGFP-fused Bub1 proteins were immunoprecipitated by GFP-Traps. Coimmunoprecipitating proteins were analyzed by SDS-PAGE and subsequent Western blotting. Ponceau is used as a loading control. WT, wild type; Mm, molecular mass; IP, immunoprecipitation.

deviation of 1.41 Å over 129 atoms. The interactions of the KI2 motif with BubR1 and of the KI1 motif with Bub1 engage equivalent interfaces located between helices α3 and α5 of the TPR assembly. Furthermore, like KI1, KI2 also adopts a helical conformation in complex with the BubR1 TPR (Fig. 5 D). Thus, there are extensive structural similarities between these two interactions (further analyzed in Fig. S2). Nevertheless, two features of the interaction of KI2 with BubR1 might explain its specificity and its apparently higher affinity with respect to the KI1–Bub1 complex. First, Arg221 of KI2 is perfectly positioned to interact with the side chains of Glu103 and Glu107 of BubR1. Asn185 of KI1, equivalent to Arg221 of KI2, does not form equally favorable contacts. Second, the bulky side chain of Phe215 of KI2 points toward the binding interface of BubR1 and appears to make favorable contacts that are likely to contribute significantly to the interaction (Fig. S2). In KI1, Thr179 substitutes for Phe215 of KI2. Its smaller side chain contributes more modestly to the binding interface.

Residues Trp125, Leu128, Cys132, Asp137, and Met138 of BubR1 occupy positions that are equivalent to those identified at the Bub1–Knl1 interface (Fig. 5, A [alignment] and E) and which have been recently shown to participate in the interaction with the KI2 region (Bolanos-Garcia et al., 2011). To probe the function of these residues in Knl1 binding, we mutated them individually into alanine and used size-exclusion chromatography to probe the interaction with Knl1(150–250) (Fig. 5 F). Individual mutations of Trp125, Leu128, Cys132, or Asp137

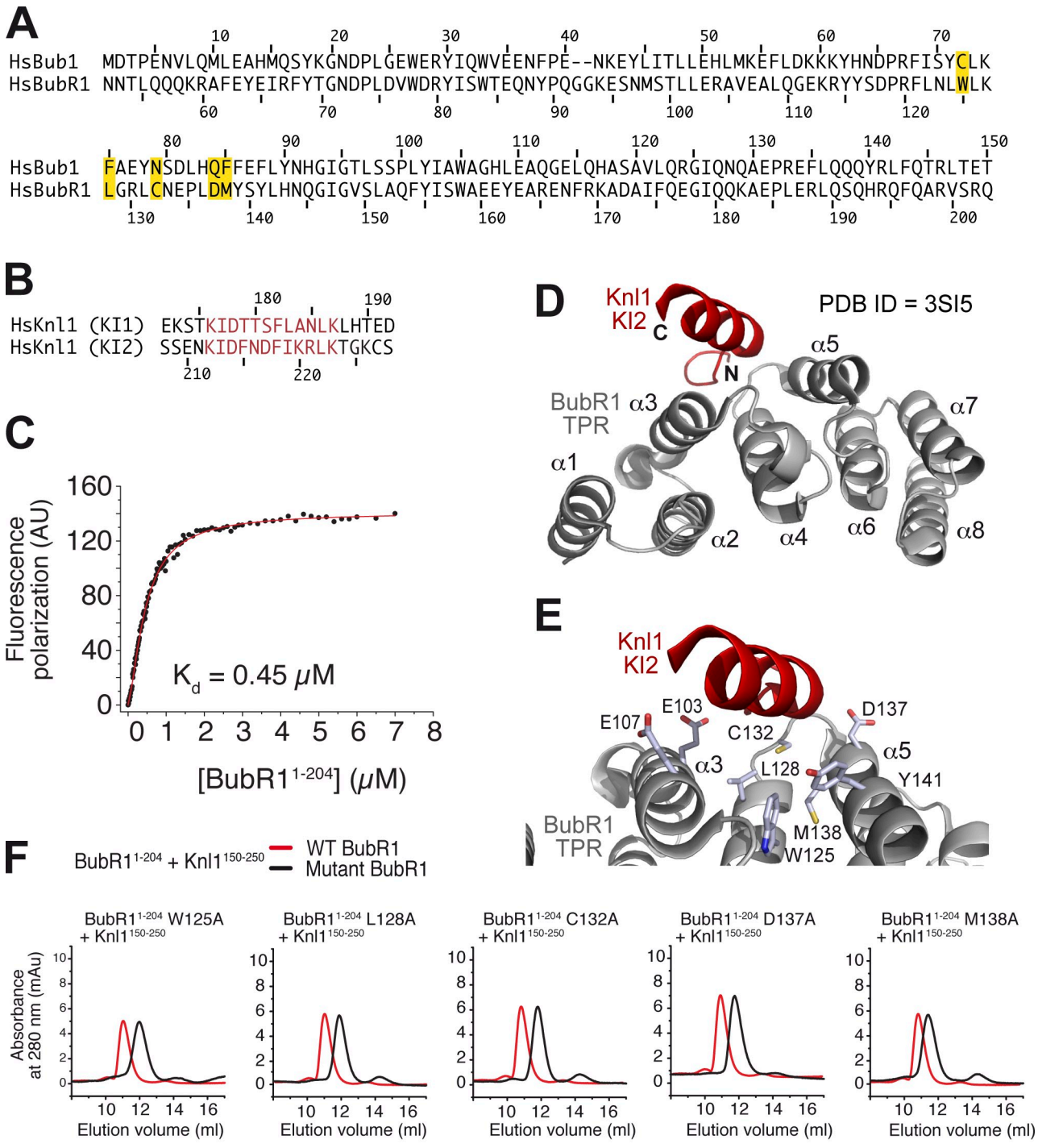

Figure 5. **Modeling and validation of the BubR1–Knl1 binding mechanism.** (A) Sequence alignment of the human Bub1 and BubR1 TPRs; residues highlighted in yellow occupy similar positions at the Knl1 interface and were mutated as discussed in the section Interaction of BubR1 with Knl1. (B) Alignment of the KI motifs of human Knl1; residues highlighted in red define the conserved binding motifs KI1 and KI2. (C) Fluorescence polarization anisotropy experiments for the interaction of a fluorescent version of Knl1(210–226) with BubR1(1–204). Red line is a fit of the data with the equation discussed in Materials and methods, Fluorescence anisotropy. AU, absorbance units. (D) The structure of the BubR1 TPRs bound to the KI2 region of Knl1 (gray and red, respectively; Protein Data Bank [PDB] accession no. 3SI5; Bolanos-Garcia et al., 2011) is displayed in the same orientation used in Fig. 3 A. The KI2 peptide is positioned on BubR1 on an interface between helices α3 and α5, like the KI1 peptide on Bub1. (E) Close-up of the structure in D from a slightly rotated view emphasizing the role of BubR1 residues implicated in Knl1 binding. (F) Elution profiles for size-exclusion chromatography runs for binding reactions of the indicated BubR1(1–204) mutants with Knl1(150–250). C, C terminus; N, N terminus.

to alanine were sufficient to disrupt the interaction with Knl1(150–250), whereas the effect of mutating Met138 was milder. Furthermore, structural analysis of the BubR1–KI2 complex shows that the side chain of this residue is partly buried (Bolanos-Garcia et al., 2011). Overall, these results demonstrate that BubR1 interacts with its cognate KI2 motif of Knl1 using a surface on the TPR that is analogous to that used by Bub1 to bind KI1.

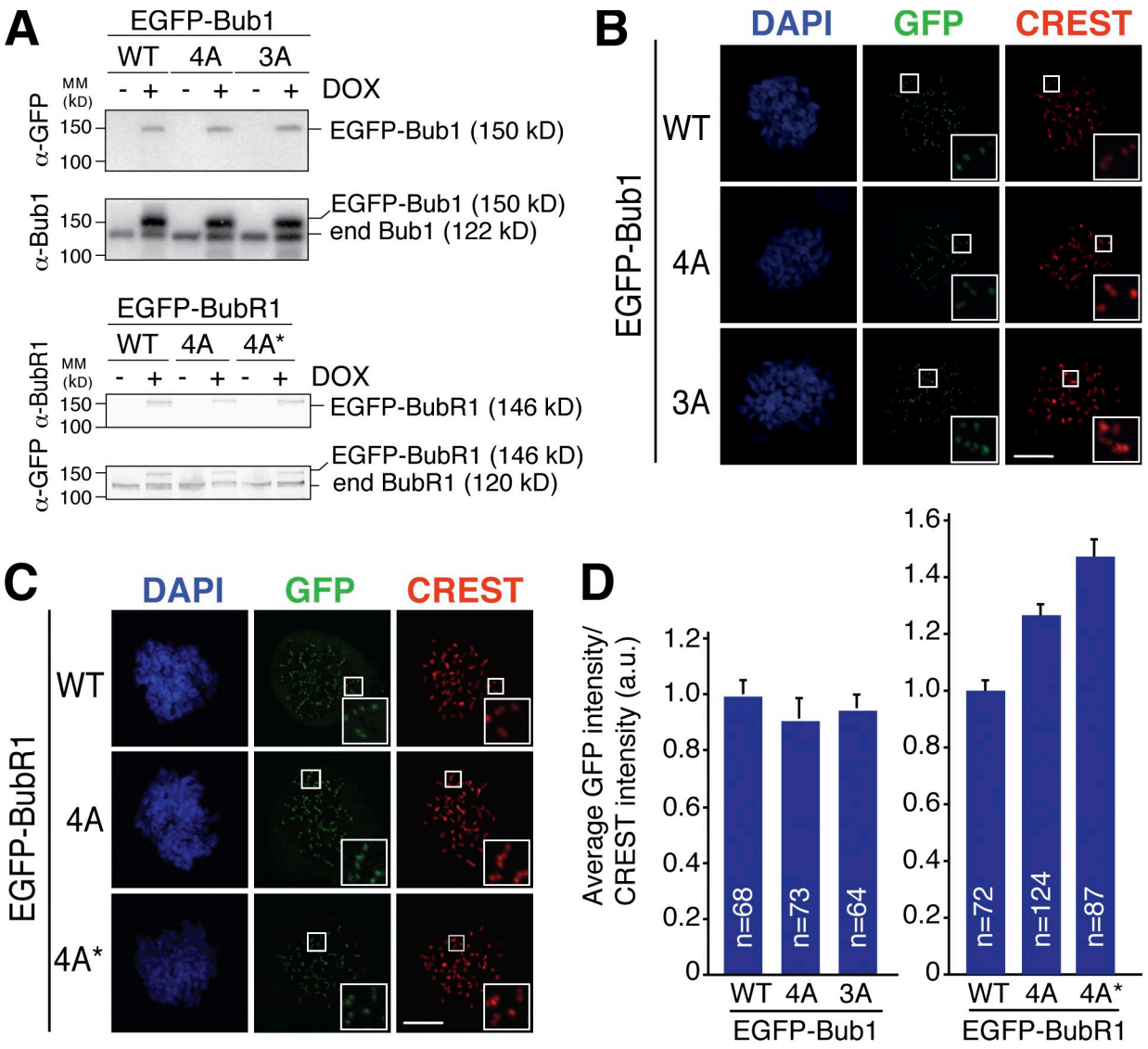

Figure 6. **Bub1 mutants impaired in Knl1 binding are recruited to kinetochores.** (A) Western blots of extracts from Flp-In T-REx cell lines expressing EGFP-tagged Bub1 (top) and BubR1 (bottom) wild type (WT) or carrying mutations in the TPR, in the absence or presence of doxycycline (DOX). Bub1(4A) and Bub1(3A) contain the F75A, N79A, Q84A, and F85A mutations and N79A, F85A, and F88A, respectively. BubR1(4A) and BubR1(4A*) contain the W125A, L128A, C132A, and D137A and W125A, L128A, C132A, and M138A mutations, respectively. End, endogenous. (B and C) Immunofluorescence of Bub1 (B) and BubR1 (C) cells treated with doxycyclin and nocodazole. Cells were stained with DAPI (DNA) and CREST sera (kinetochores). Insets show a higher magnification of kinetochore regions (boxes). Bars, 5 µm. (D) Graphs showing the mean GFP intensity of kinetochores in cells used in B (left) and C (right) normalized to the mean GFP intensity of wild-type signals. *n* indicates the numbers of measured kinetochores. Error bars indicate SEM. a.u. arbitrary unit; MM, molecular mass.

Knl1 binding and kinetochore recruitment of Bub1 and BubR1

Results in Fig. 1 demonstrate that the N-terminal TPR regions of Bub1 and BubR1 are not sufficient for kinetochore recruitment. More surprisingly, the results also suggest that these regions might not even be strictly necessary for kinetochore recruitment. A possible conclusion from this analysis is that the interaction of the Bub1 and BubR1 TPR with the Knl1 (150–250) region might not be essential for kinetochore recruitment of these checkpoint kinases.

As explained in section The TPR domains of Bub1 and BubR1 bind Knl1 directly, the characterization of Knl1-binding interfaces on Bub1 and BubR1 allowed us to probe the role of Knl1 binding in kinetochore recruitment of these proteins in the context of the full-length protein, i.e., without resorting to deletion mutants that might disrupt hypothetical intramolecular regulatory steps. We therefore tested the ability of EGFP fusions of Bub1 or BubR1 mutants carrying multiple alanine substitutions on their KI1 or KI2 binding sites, respectively (described in the legend of Fig. 6 and abbreviated as Bub1(3A), Bub1(4A), BubR1(4A), and BubR1(4A)*) or of individual alanine point mutants (Fig. S3, A and B) to be recruited to kinetochores.

We thus generated stable doxycycline-inducible HeLa cell lines. After a 24-h treatment with doxycycline, EGFP-tagged proteins were expressed at comparable levels that equaled or slightly exceeded the levels of endogenous Bub1 or BubR1 (Fig. 6 A). As for the case of the N-terminal deletion mutants,

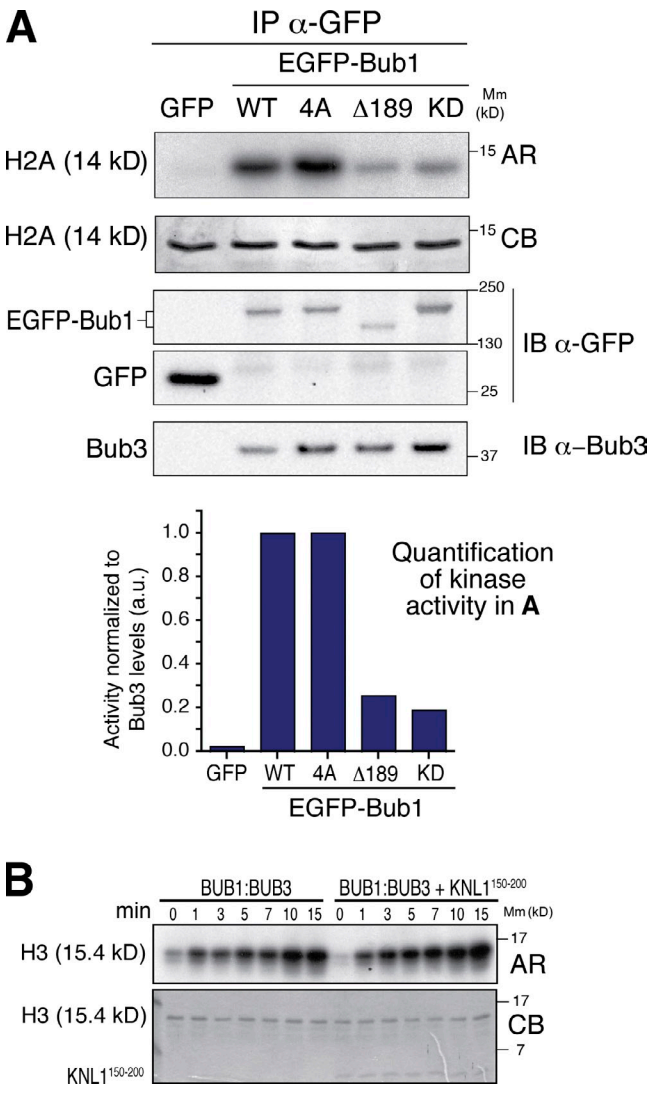

Figure 7. **Deletion of the TPR region represses Bub1 kinase activity.** (A) In vitro kinase activity of anti-EGFP immunoprecipitates of EGFP and the indicated EGFP-fused Bub1 proteins from Flp-In T-REx cell lines. Kinase activity was tested on histone 2A (H2A) as a substrate; KD, kinase dead, carrying K821R mutation; AR, autoradiography; CB, Coomassie brilliant blue; a.u., arbitrary unit. The quantification data shown are from a single representative experiment out of two repeats. (B) A time course of H3 phosphorylation in the presence of the recombinant Bub1–Bub3 complex, in the absence (left) or in the presence (right) of Knl1(150–200). IB, immunoblot; Mm, molecular mass; WT, wild type.

kinetochore recruitment of Bub1(3A) or Bub1(4A) was not affected; recruitment of the two variants of BubR1(4A) was increased relative to the wild-type control (Fig. 6, B–D). As a further control, and to exclude any possible effect from endogenous Bub1, we assessed kinetochore recruitment of EGFP-Bub1 proteins in HeLa cells in which we had previously depleted Bub1 by RNAi (Fig. S3, C–E). Also in this case, we observed normal kinetochore recruitment of Bub1(4A) and Bub1(Δ189). Overall, these observations confute the hypothesis that the interaction of the TPR regions of Bub1 and BubR1 with the KI motifs of Knl1 regulates intra- or intermolecularly the degree of exposure of a kinetochore-binding region located elsewhere in the sequence of Bub1 or BubR1. On the contrary, the data strongly suggest that the TPR regions of Bub1 and BubR1 play a marginal role in kinetochore recruitment of Bub1 and BubR1.

Effects of the TPR region on the kinase activity of Bub1

To investigate alternative functions of the TPR region, we asked whether it influenced the catalytic activity of Bub1. Various EGFP-Bub1 constructs were expressed in stable doxycycline-inducible HeLa cell lines, partially purified via EGFP immunoprecipitation, and tested in kinase assays with H2A as a substrate. To assess the specificity of Bub1 activity in our immunoprecipitates, we first confirmed that the activity of a recombinant version of Bub1–Bub3 purified from insect cells was inhibited with 5 µM 2OH-BNPP1, a small-molecule inhibitor of Bub1 (Fig. S4 A; Kang et al., 2008). Next, we added 2OH-BNPP1 to a kinase assay reaction with immunoprecipitated Bub1 and found levels of inhibition comparable with those observed with the recombinant kinase (Fig. S4 B). These experiments testify to the specificity of the kinase assay. As an additional control, we tested the effects of mutations in the active site of the recombinant Bub1–Bub3 kinase (Fig. S4 C).

Next, we tested the H2A kinase activity of immunoprecipitates of cycling cells expressing similar amounts of EGFP-Bub1 or its variants, including Bub1(4A), Bub1(Δ189), and a kinase-dead mutant (Bub1(KD); Fig. S4 D). Deletion of the TPR region decreased the kinase activity of Bub1 to levels comparable with those of the kinase-dead mutant (Fig. 7 A). On the other hand, the catalytic activity of Bub1(4A) was unaffected in this assay, suggesting that the ability of this domain to bind Knl1 might not be essential for Bub1 kinase activity and that the determinants required for activity map elsewhere in the TPR region. Essentially identical results were obtained when using H3 (histone 3) as a substrate (unpublished data). In agreement with the idea that the interaction with Knl1 does not modulate the catalytic activity of the Bub1–Bub3 complex, the H3 kinase activity of recombinant Bub1–Bub3 purified from insect cells was not affected by the addition of a recombinant Knl1(150–200) segment (Fig. 7 B).

Identification of the minimal kinetochore-binding domain of Bub1

We tried to identify a minimal kinetochore-binding domain of Bub1. In Fig. 1, we demonstrated that residues 190–436, from which the TPRs of Bub1 are excluded, might be necessary for kinetochore recruitment of Bub1. To test whether this region is also sufficient for kinetochore recruitment, we generated a construct encompassing Bub1 residues 190–447. In agreement with the idea that this region of Bub1 is sufficient for kinetochore localization, EGFP-Bub1(190–447) localized normally at the kinetochore (Fig. S5 A). Although Bub1(1–150) failed to localize at kinetochores, inclusion of a C-terminal segment that included the Bub3-BD of Bub1 (Bub1(1–284)) led to robust kinetochore recruitment (Fig. S5 A). These results indicate that a segment comprised between residues 190 and 284 of human Bub1 is sufficient for kinetochore recruitment, in agreement with a previous study (Taylor et al., 1998).

Next, we refined our analysis of this interaction by expressing additional constructs, including Bub1(209–270) and Bub1(227–270). The latter construct matched almost exactly the segment of budding yeast Bub1 that was previously cocrystallized with Bub3 (Larsen et al., 2007), whereas the former is preceded by an 18-residue N-terminal extension of unknown function (Fig. 8 A, alignment). Although Bub1(209–270) localized robustly to kinetochores, Bub1(227–270) was unable to reach kinetochores (Fig. 8 B and Fig. S5 B for expression levels). These results suggest that efficient kinetochore recruitment requires the Bub3-BD and a short N-terminal extension.

To test the importance of the Bub3-binding region, we mutated Glu248 of Bub1, a residue previously shown to be essential for the interaction of Bub1 with Bub3 (Larsen et al., 2007), into lysine (E248K, referred to as EK mutant) in the context of the Bub1(209–270) construct and expressed it in HeLa cells (Fig. S5 C shows expression levels). As expected, the mutation abolished kinetochore recruitment of the Bub1(209–270) construct, demonstrating that binding to Bub3 is essential for kinetochore localization of Bub1 (Fig. 8 C). Moreover, the E248K mutation did not have additional effects on kinetochore localization in the context of Bub1 (227–270) (Fig. S5, D and E).

To assess whether the N-terminal segment of the Bub1 (209–270) construct shown to be necessary for kinetochore recruitment is also important for the interaction with Bub3, we expressed GFP fusion proteins of Bub1(209–270), Bub1 (227–270), and Bub1(227–270-EK) in HeLa cells and quantified the abundance of Bub3 in the resulting anti-GFP immunoprecipitates (Fig. 8 D). We observed a strong correlation between the strength of Bub3 binding by the different constructs and their interaction with kinetochores, in agreement with the results from localization experiments (Fig. 8 B and Fig. S5 D). This result supports the idea that Bub3 binding is essential for the interaction of Bub1 with kinetochores. This idea was further emphasized by robust coprecipitation of at least two kinetochore subunits, Knl1 and Hec1, with Bub1(209–270), a construct that binds Bub3 with high affinity (Fig. 8 D). Similarly, the interaction of Bub1 with BubR1 appeared to correlate with the ability of Bub1 to bind Bub3 (Fig. 8 D). Conversely, Bub1(227–270) and Bub1(227–270-EK), which bind poorly to Bub3, did not interact robustly with kinetochores or BubR1.

Discussion

Structural analysis of Bub1, a 1,085-residue multidomain protein, has so far revealed the organization of the kinase domain (Kang et al., 2008), the TPR region (Bolanos-Garcia et al., 2009; D'Arcy et al., 2010), and of the Bub3-BD in complex with Bub3 (Larsen et al., 2007). Here, we extend these previous analyses by elucidating the structure of the complex of the Bub1 TPRs with its cognate KI1 motif of Knl1. The Knl1-binding interface is located on the convex surface of the TPRs. Our structure is equivalent to the crystal structure of the BubR1 TPRs bound to the KI2 region of Knl1, which was reported while this paper was under review (Bolanos-Garcia et al., 2011). Based on current structural knowledge on the interaction of helical repeats with their protein ligands, this is unusual but not unprecedented. For instance, the *S. cerevisiae* protein Caf4 interacts both on the concave and convex surface of the TPRs of Fis1 (Protein Data Bank accession no. 2PQR; Zhang and Chan, 2007).

It is plausible that the regulation of the catalytic output of Bub1 at kinetochores is mediated by complex intramolecular conformational changes triggered by kinetochores. Structural analysis of the kinase domain of Bub1, which revealed an intramolecular inhibitory switch that must be relieved for full kinase activation, lends support to this hypothesis (Kang et al., 2008). Our observations show that the N-terminal region of Bub1 influences the catalytic output of the kinase domain at the opposite end of the primary structure but that this effect might not depend on the KI1-binding interface (Fig. 7 A). In the future, we will try to clarify whether this occurs by releasing the previously identified intramolecular inhibitory mechanism (Kang et al., 2008). Furthermore, we show that the interaction of Bub1 with Bub3, and therefore presumably with kinetochores, is important to mediate the interaction of Bub1 with BubR1. Future studies will have to address the precise molecular mechanism through which these effects take place. Eventually, these studies will illuminate the detailed molecular mechanism of activation of Bub1, and possibly of BubR1, at the kinetochore.

By showing that the Bub3-binding region of Bub1, rather than the TPRs, is essential for kinetochore recruitment, our analysis resolves an open controversy, and it lends support to original studies indicating that the Bub3-BD of Bub1 (Taylor et al., 1998), later renamed (less informatively) as GLEBS motif (Wang et al., 2001), is necessary and sufficient for kinetochore recruitment of Bub1. The previously described deleterious effects on kinetochore localization of the mutations Leu122 to Gly (L122G, already mentioned in the Introduction; Kiyomitsu et al., 2007) might be an unexpected consequence of the destabilization of the hydrophobic core of the TPR region, where the side chain of Leu122 is located.

Impairment of the interaction of the Bub1 TPRs with the KI motif is, in principle, expected to reduce the kinetochore-binding affinity of Bub1. But the extent of this effect, if at all existing, is insufficient to alter the levels of kinetochore Bub1 significantly. With the goal of identifying subtle differences in the dynamics of kinetochore residence of Bub1 or of the Bub1 mutants incapable of binding Knl1, we performed FRAP experiments. These experiments, however, failed to reveal significant differences in recovery rates between Bub1(WT) and the Bub1(4A) mutant impaired in Knl1 binding (unpublished data).

Our analysis of the requirements for recruiting BubR1 to kinetochores is also in line with previous studies showing that BubR1(1–203) or BubR1(1–363) is unable to reach kinetochores, whereas a BubR1(357–1,052) construct localizes apparently normally (Malureanu et al., 2009; Elowe et al., 2010). When considered together, therefore, the available evidence supports the unifying theme that the TPR regions of Bub1 and BubR1 are both dispensable for kinetochore recruitment. At least in the case of Bub1, its Bub3-binding region, likely through concomitant interactions of Bub3 with currently unknown

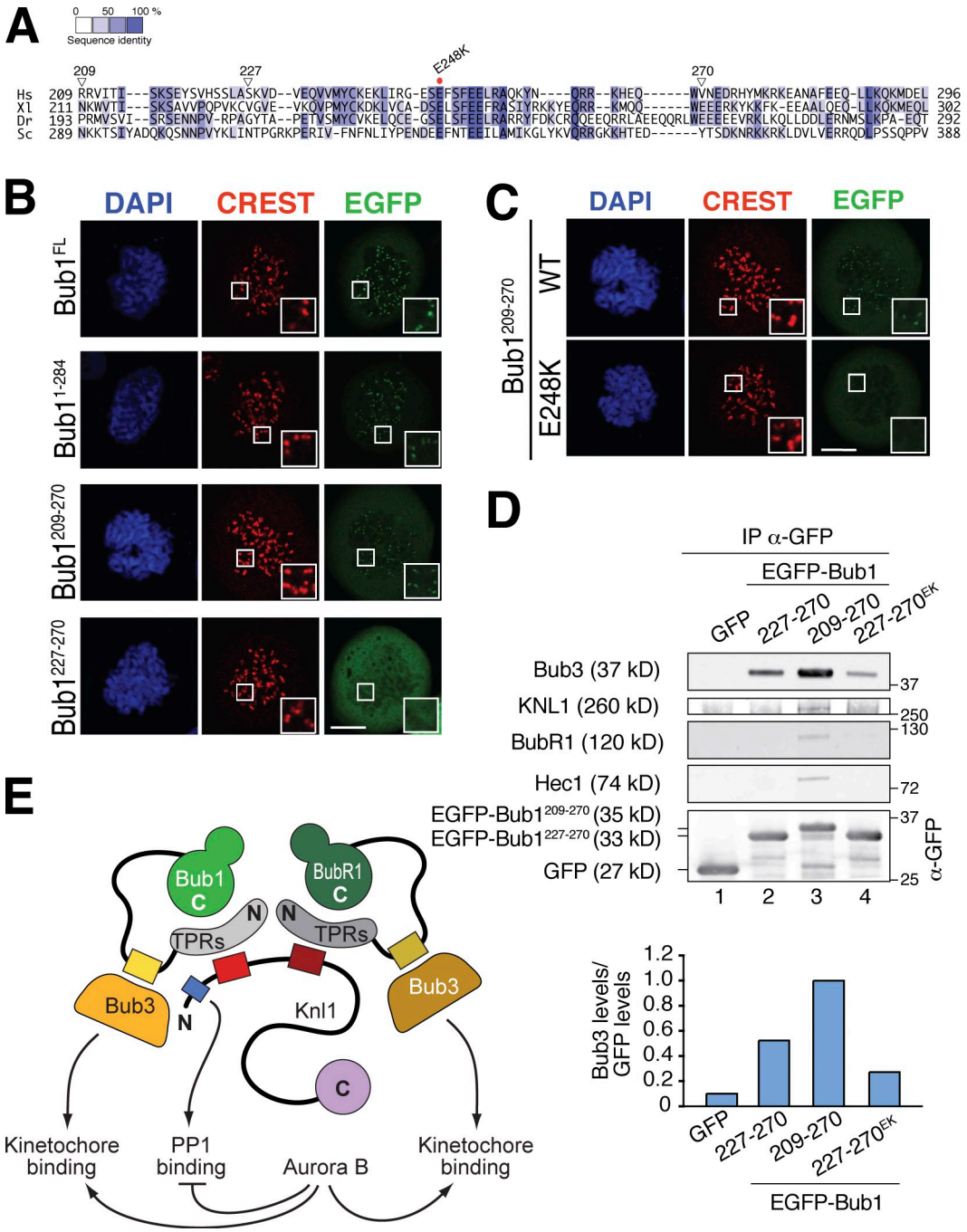

Figure 8. **Minimal kinetochore-binding domain and the role of the TPR region.** (A) Sequence alignment of the Bub3-binding region of Bub1 (Hs, *Homo sapiens*; Xl, *Xenopus laevis*; Dr, *Danio rerio*; Sc, *S. cerevisiae*. (B) Fluorescence images of mitotic HeLa cells expressing the indicated EGFP-Bub1 constructs and treated with nocodazole. Cells were stained with DAPI (DNA) and CREST sera (kinetochores). Insets show a higher magnification of kinetochore regions (boxes). (C) Immunofluorescence images of mitotic HeLa cells expressing the EGFP-tagged fragments of the Bub3-BD of Bub1 and carrying the E248K mutation (EK). Cells were treated as in B. Note that the E248K mutation abolished the localization of EGFP-Bub1(209–270). The data in B and C derive from a single experiment, and the same image for the Bub1(209–270) construct is shown in B and C. (D) Immunoprecipitation of EGFP-tagged Bub1 proteins. HeLa cells were transfected with the corresponding plasmids and treated with 330 nM nocodazole for 16 h. (top) Coimmunoprecipitating proteins were analyzed by SDS-PAGE and Western blotting. On the bottom, a graph showing the quantification of Bub3 levels at the top normalized to the corresponding GFP levels and normalized to the value of Bub1(209–270). The quantification data shown are from a single representative experiment out of two repeats. (E) Models of Bub1 and BubR1 kinetochore recruitment. Bub1 and BubR1 have similar domain structures, and it is plausible that they interact with kinetochores through partly related mechanisms. The interaction of Bubs with the Bub3-BD (yellow boxes) is crucial for kinetochore recruitment. The TPRs of Bub1 and BubR1 interact with the KI1 and KI2 motifs of Knl1, respectively. This interaction is important for the ability of Bub1 to bind BubR1 possibly because Knl1 acts as a scaffold for recruiting both proteins. The PP1-binding motif of Knl1 is negatively regulated through Aurora B phosphorylation. Aurora B, on the other hand, facilitates the interaction of Bub1 and BubR1 with kinetochores. N, N terminus; C, C terminus; WT, wild type. Bars, 5 µm.

targets, contributes the bulk of the binding affinity required for kinetochore binding (Fig. 8, B–D). A previous study making use of a 42-residue deletion in the Bub3-BD of BubR1 indicates that this might be true also for BubR1 (Taylor et al., 1998).

Identification of the kinetochore targets that mediate the interaction of Bub1 and BubR1 with kinetochores is of crucial importance. Knl1 is required for kinetochore recruitment of Bub1 and BubR1 (Kiyomitsu et al., 2007; Pagliuca et al., 2009). Because the interaction of Bub1 with the KI motifs of Knl1 is insufficient for kinetochore recruitment, it is plausible that at least another segment of Knl1 is involved, possibly through an interaction with the Bub3-binding region of Bub1 and with Bub3. This is in line with findings that Bub1 and Bub3 may be reciprocally required for efficient kinetochore recruitment (Taylor et al., 1998; Sharp-Baker and Chen, 2001; Chen, 2002; Meraldi et al., 2004; Vigneron et al., 2004; Logarinho et al., 2008). An important conclusion from our analysis is that the integrity of the Bub3-binding region of Bub1 is important for the interaction of Bub1 with BubR1 and with kinetochores (Fig. 8 D).

The precise molecular mechanism underlying the interaction of Bub1–Bub3 with BubR1–Bub3 and with kinetochores is currently unclear (Fig. 8 E). Kinetochores are very complex and dynamic assemblies, whose most intriguing feature is the ability to regulate checkpoint signaling as a function of the progression of kinetochore–microtubule attachment. The feedback mechanisms that couple the maturation of kinetochore–microtubule attachment to checkpoint control are known only imperfectly. The Mad1–Mad2 complex, which plays an essential role in Mad2 activation at the kinetochore (De Antoni et al., 2005), is progressively removed from kinetochores via a dynein-dependent pathway (Howell et al., 2001; Wojcik et al., 2001; Gassmann et al., 2008). Forced retention of Mad1–Mad2 at kinetochores prevents checkpoint satisfaction despite the formation of a normal metaphase plate (Maldonado and Kapoor, 2011a). Thus, the removal of at least a subset of the checkpoint proteins from the kinetochore is a prerequisite for exiting mitosis.

Bub1 is also progressively removed from kinetochores upon microtubule attachment (Taylor et al., 2001; Famulski and Chan, 2007). How this is achieved at the molecular level is not known but worthy of further investigations. A fundamental emerging concept is that the KMN network complex plays a crucial role in relaying kinetochore–microtubule attachment to checkpoint silencing. This idea is corroborated by the observation that the KMN acts not only as the crucial microtubule-binding moiety of the kinetochore but also as a recruitment platform for all known checkpoint proteins, excluding Aurora B (Santaguida and Musacchio, 2009). It is therefore from this platform that the checkpoint proteins have to be removed for checkpoint silencing to be achieved.

The Knl1 subunit is probably a focal point of this dynamic regulation. In the immediate vicinity of the Bub1 KI1 motif, Knl1 contains a bipartite binding region for the PP1 phosphatase (Fig. 1 A and Fig. 8 E; Liu et al., 2010). This region has also been implicated in microtubule binding (Pagliuca et al., 2009; Welburn et al., 2010). The RRVSF motif in the PP1-binding region is a target of the Aurora B kinase, and Aurora B phosphorylation antagonizes PP1 binding, limiting the timing of its kinetochore recruitment to the final phases of kinetochore–microtubule attachment (Wu et al., 2009; Liu et al., 2010). Failure to recruit the PP1 phosphatase results in a metaphase arrest with an active spindle checkpoint (Maldonado and Kapoor, 2011b; Rosenberg et al., 2011). In the future, it will be important to investigate this complex network of interactions and if and how Bub1 recruitment to Knl1 impinges on the opposition of Aurora B and PP1.

Materials and methods

Mammalian plasmids

All the plasmids (except the one used in Fig. S1) were derived from the pcDNA5/FRT/TO vector (Invitrogen). The control plasmid for EGFP expression was created by PCR amplifying the EGFP sequence from pEGFP-C1 (Takara Bio Inc.) and cloning it into the pcDNA5/FRT/TO vector previously modified to carry an internal ribosomal entry site (IRES) sequence to obtain the pcDNA5/FRT/TO EGFP-IRES vector. To create all N-terminal EGFP-Bub1 plasmids, Bub1 sequences were obtained by PCR amplification from a pEGFP-C1 vector containing RNAi-resistant Bub1 (a gift from M. Yanagida, University of Kyoto, Kyoto, Japan) and subcloned into the pcDNA5/FRT/TO EGFP-IRES vector. To create the BUB1(Δ189)-EGFP fusion used in Fig. S1, the Bub1 sequence was PCR amplified and cloned into pEGFP-N1 (Takara Bio Inc.). All Bub1 constructs were RNAi resistant (Kiyomitsu et al., 2007). To create all N-terminal EGFP fusions, BubR1 sequences were amplified by PCR and cloned in frame with the EGFP tag in the pcDNA5/FRT/TO EGFP-IRES vector. Site-directed mutagenesis was performed with a mutagenesis kit (QuikChange; Agilent Technologies) to generate single and multiple mutants in the Bub1 and BubR1 constructs. pcDNA5/FRT/TO-based plasmids were used for both transient transfection and to generate stable inducible cell lines. All plasmids were checked by DNA sequencing.

Cell culture and transfection

HeLa cells were grown in DME (EuroClone) supplemented with 10% FBS (Hyclone) and 2 mM L-glutamine. Nocodazole (Sigma-Aldrich) was used at a concentration of 3.3 µM unless differently specified. 2 mM thymidine was purchased from Sigma-Aldrich. For all plasmid transfections of HeLa cells, transfection agent (FuGENE 6; Roche) was used at a 3:1 ratio with plasmid DNA. Cells were analyzed 36–68 h after transfection.

Flp-In T-REx HeLa cells used for stable doxycycline-inducible cell lines were a gift from S.S. Taylor (University of Manchester, Manchester, England, UK). Flp-In T-REx HeLa host cell lines were maintained in DME with 10% tetracycline-free FBS (Invitrogen) supplemented with 50 µg/ml Zeocin (Invitrogen). Flp-In T-REx HeLa expression cell lines were generated as previously described (Screpanti et al., 2011). In brief, Flp-In T-REx HeLa host cells were cotransfected with a ratio of 9:1 (wt/wt) pOG44/pcDNA5/FRT/TO expression plasmid using transfection agent (FuGENE6). 48 h after transfection, Flp-In T-REx HeLa expression cell lines were put under selection for 2 wk in DME with 10% tetracycline-free FBS supplemented with 250 µg/ml hygromycin (Roche) and 5 µg/ml blasticidin (MP Biomedicals). The resulting foci were pooled and tested for expression. Gene expression was induced with 0.5 µg/ml doxycycline (Sigma-Aldrich) for 24 h. To generate mitotic populations of these cells used in 4D, cells were treated with 330 nM nocodazole for 16 h. Mitotic cells were then harvested by shake off.

RNAi

Bub1 siRNA duplexes had the sequence 5′-GGUUGCCAACACAAGUUCU-3′ and were purchased from Thermo Fisher Scientific. To perform RNAi, 50 nM Bub1 siRNA duplexes were transfected using Lipofectamine 2000 reagent (Invitrogen) according to the manufacturer's instructions. After 5 h from transfection of siRNA duplexes, cells were synchronized with a double thymidine arrest. In brief, cells were washed with PBS, treated with thymidine for 16 h, and then released into fresh medium. 3 h after the release, 50 nM siRNA duplexes were transfected again. After 5 h from transfection of siRNA duplexes, cells were treated with thymidine for 16 h and released in fresh medium.

Immunoprecipitation and immunoblotting

Cells were lysed in lysis buffer (150 mM KCl, 75 mM Hepes, pH 7.5, 1.5 mM EGTA, 1.5 mM $MgCl_2$, 10% glycerol, and 0.075% NP-40 supplemented

with protease inhibitor cocktail [Protease Inhibitor Cocktail Set III; EMD]) and phosphatase inhibitors (PhosSTOP; Roche). For immunoprecipitation experiments, extracts were precleared with a mixture of protein A–Sepharose (CL-4B; GE Healthcare) and protein G–Sepharose (rec-Protein G-Sepharose 4B Conjugate; Invitrogen) for 1 h at 4°C and centrifuged for 4 min at 4,000 rpm. Supernatants were then incubated with GFP-Traps (ChromoTek; 3 µl/mg of extract) for 2–4 h at 4°C. Immunoprecipitates were washed with lysis buffer and resuspended in sample buffer, boiled at 95°C for 5 min, and analyzed by SDS-PAGE and Western blotting.

The following antibodies were used for immunoblotting: anti-Actin (mouse monoclonal antibody AC-40; Sigma-Aldrich; working dilution of 1:1,000), anti-GFP (in house made rabbit polyclonal antibody; working dilution of 1:400), anti-GFP (mouse monoclonal B-2, 9996; Roche; working dilution of 1:1,000), anti-Hec1 (human Ndc80; mouse clone 9G3.23; GeneTex, Inc.; working dilution of 1:1,000), anti-Mis12 (in house made mouse monoclonal antibody; clone Q015; working dilution of 1:5), anti-KNL1 (in house made rabbit polyclonal SI0788 antibody; working dilution of 1:1,000), anti-Bub1 (rabbit polyclonal Ab9000; Abcam; working dilution of 1:5,000), anti-BubR1 (mouse; BD; working dilution of 1:1,000), mouse anti-Bub3 (mouse; BD; working dilution of 1:1,000), antivinculin (mouse monoclonal antibody; clone hVIN-1; Sigma-Aldrich; working dilution of 1:100,000), antiphospho–S10-H3 (rabbit polyclonal 06–570; Millipore; working dilution of 1:1,000). For Fig. 4 D, Fig. 6 A (top), and Fig. 7 A, blots were incubated with anti–mouse and anti–rabbit affinity-purified secondary antibodies with horseradish peroxidase conjugate (Bio-Rad Laboratories; working dilution of 1:10,000) detected with a Western blotting system (ECL; GE Healthcare) with films or digital imaging (ChemiBIS 3.2; DNR Bio-Imaging Systems). All other blots were incubated with anti–mouse and anti–rabbit IRDye 680LT or IRDye 800CW secondary antibodies obtained from LI-COR Biosciences (working dilution of 1:10,000) and scanned with Odyssey 3.0 (LI-COR Biosciences).

Immunofluorescence

HeLa cells were plated onto coverslips pretreated with 15 µg/ml poly(D)lysine (Sigma-Aldrich). The day after, cells were transfected with the plasmids for 48–68 h and treated with nocodazole for 6–10 h. Immunofluorescence was performed as described previously (Screpanti et al., 2011). Anticentromeric antibody (working dilution of 1:60 diluted in 2% BSA-PBS; Antibodies, Inc.) was incubated for 2 h to stain kinetochores. Anti–human Cy3- or DyLight 649–conjugated secondary antibodies (Jackson ImmunoResearch Laboratories, Inc.) were diluted at 1:100 in BSA 2%–PBS and incubated for 30 min. DAPI was used to stain the DNA. Coverslips were then mounted with Mowiol mounting media. Cells were imaged at room temperature using a confocal microscope (TCS SP2; Leica) equipped with a 63×, NA 1.4 objective lens using the LCS 3D software (Leica). Images in Fig. S3 (A and B) were acquired as z sections at 0.2442 µm and converted into maximal intensity projections using ImageJ (National Institutes of Health). Intensities of kinetochore areas, from at least four cells per condition, were measured with ImageJ software and corrected for the mean intensity of nonkinetochore areas. Measurements were graphed with Excel (Microsoft) software.

In vitro kinase assays

Recombinant His-Bub1–Bub3 wild-type and kinase-dead kinases were expressed and purified from Sf9 insect cells infected with recombinant baculoviruses as previously described (Santaguida et al., 2010). In brief, Sf9 insect cells infected with recombinant baculoviruses were lysed in lysis buffer (50 mM Tris, pH 8.0, 300 mM NaCl, 5% glycerol, 1 mM β-mercaptoethanol, and protease inhibitors [Protease Inhibitor Cocktail Set III, Calbiochem]). The complex was isolated on Ni-nitrilotriacetic acid beads, eluted with 200 mM imidazole, dialyzed in 10 mM Tris HCl, pH 8.0, 100 mM NaCl, 5% glycerol, and 1 mM DTT, and further purified by size-exclusion chromatography. Full-length H2A of *Xenopus laevis* was expressed in *E. coli*, purified under denaturing conditions, and refolded for being used as Bub1 in vitro substrate following the original protocol (Luger et al., 1997) with small modifications. In brief, the bacterial lysate was spun for 30 min at 4°C at 25,000 *g* twice. The inclusion body containing the pellet was then subjected to chemical lysis by adding 1 ml DMSO for 30 min at room temperature followed by adding 30 ml of unfolding buffer (7 M guanidinium HCl, 20 mM Tris-HCl, pH 7.5, and 10 mM DTT) and incubated for 1 h at room temperature. Cell debris was removed by centrifugation at 4°C at 25,000 *g*. The supernatant containing the unfolded proteins was dialyzed thoroughly against 7 M urea, 200 mM sodium chloride, 20 mM Tris, pH 7.4, and 5 mM 2-mercaptoethanol at 4°C. The dialyzed supernatant was then loaded onto a column (HiPrep SP FF 16/10 GE Healthcare), and the histone H2A was eluted with a linear gradient in high salt buffer (7 M urea, 2 M sodium chloride, 20 mM Tris, pH 7.4, and 5 mM 2-mercaptoethanol). Histone H2A–containing fractions were then dialyzed first against 2 M NaCl, 10 mM Tris-HCl, pH 7.5, and 5 mM DTT and finally against 200 mM NaCl, 10 mM Tris-HCl, pH 7.5, and 1 mM DTT to achieve fully refolded conditions.

Kinase assays were performed in 30 µl reaction volume as described previously (Santaguida et al., 2010). In brief, reaction mixes contained 50 µM ATP, 1 mM DTT, phosphatase inhibitor cocktail (Sigma-Aldrich), 10 µCi γ-[^{32}P]ATP, and 10 µM H2A histone as a substrate. His-Bub1–Bub3 kinases were used at a concentration of 50 nM diluted in kinase buffer (50 mM Tris-HCl, pH 7.6, 150 mM NaCl, 10 mM $MgCl_2$, and 1 mM EDTA). 2OH-BNPP1 inhibitor (a gift from K. Shokat, University of California, San Francisco, San Francisco, CA) was used at a final concentration of 5 µM. Knl1(150–250) peptide was expressed and purified as described in Protein expression and purification and used at the final concentration of 1.8 µM. For kinase immunoprecipitation followed by kinase assay, Flp-In T-REx cells were induced with doxycycline (see Cell culture and transfection) and lysed in lysis buffer (150 mM KCl, 75 mM Hepes, pH 7.5, 1.5 mM $MgCl_2$, 10% glycerol, and 0.075% NP-40 supplemented with protease inhibitors cocktail [Protease Inhibitor Cocktail Set III]) and phosphatase inhibitors (PhosSTOP). Immunoprecipitation was performed as described in Immunoprecipitation and immunoblotting. Kinase reaction mixes were added to the immunoprecipitates, previously washed with kinase buffer, incubated for 1 h at 30°C, and quenched with SDS loading buffer. Proteins were resolved on a 14% SDS-PAGE. Incorporation of ^{32}P was visualized by autoradiography.

Protein expression and purification

Sequences encoding Bub1(1–150), BubR1(1–204), Knl1(150–200), Knl1(201–250), and Knl1(150–250) were created by PCR amplification and subcloned in the first cassette of pGEX-6P-2rbs (Sironi et al., 2001). Site-directed mutagenesis was performed with a mutagenesis kit (QuikChange) and used to generate mutants in the Bub1 and BubR1 expression constructs. All constructs were verified by sequencing.

Bacterial strain *E. coli* BL21(DE3)pLysS was used for expression of Bub1 and BubR1 constructs. Rosetta strain was used for expression of Knl1 constructs. To express Bub1(1–150), BL21 cells were grown in Luria-Bertani medium at 37°C until an OD_{600} of ∼0.7. At this point, expression was induced with 0.3 mM IPTG, and cells were cultured at 20°C for 16 h before collection. The BubR1(1–204) construct was expressed in BL21(DE3)pLysS cells. Expression was induced with 0.2 mM IPTG at an OD_{600} of ∼0.7, and cells were further cultured at 25°C for 16 h. Rosetta cells carrying expression plasmids for Knl1(150–200), Knl1(201–250), or Knl1(150–250) were grown in Luria-Bertani medium at 37°C. Expression was induced with 0.3 mM IPTG at an OD_{600} ∼0.8, and cells were cultured at 22°C for 16 h before collection by centrifugation.

Cell pellets were resuspended in lysis buffer (50 mM Tris, 0.5% NP-40, 150 mM NaCl, 2 mM EDTA, and 1 mM DTT, pH 7.4) supplemented with protease inhibitor cocktail (Protease Inhibitor Set III). After sonication, the cell lysate was cleared by high-speed centrifugation. The supernatant was collected and incubated with glutathione Sepharose 4 Fast Flow beads (GE Healthcare) at room temperature for 2 h. The Sepharose beads bound with GST-tagged protein constructs were collected by centrifugation and washed with 20 bed volumes PBS buffer followed by 5 bed volumes protease cleavage buffer (PreScission; 50 mM Tris, 150 mM NaCl, 1 mM EDTA, and 1 mM DTT). The beads were incubated with PreScission protease at a 200:1 ratio (estimated recombinant protein w/protease w) at 4°C overnight. The collected eluate was applied to a column (Superdex 75 10/300; GE Healthcare) equilibrated in size-exclusion chromatography buffer (10 mM Na-phosphate and 150 mM NaCl, pH 7.4). Size-exclusion chromatography was performed at a flow rate of 0.5 ml/min, and the fractions containing target proteins were collected, concentrated, flash frozen in liquid N_2, and stored at −80°C.

Analytical size-exclusion chromatography

Analytical size-exclusion chromatography experiments were performed on a column (Superdex 75 10/300). All samples were eluted at 4°C in size-exclusion chromatography buffer at a flow rate of 0.5 ml/min. Elution of proteins was monitored at 280 nm. To detect complex formation, different combination of proteins were mixed at a concentration of 5 µM in 600 µl, incubated at 4°C for >1 h, and then subjected to chromatography. Fractions were collected and analyzed by SDS-PAGE and Coomassie staining.

Fluorescence anisotropy

Fluorescence anisotropy measurements were performed with a microplate reader (Infinite F200; Tecan) at 20°C. Fluorescein (5-FAM)-labeled Knl1(174–190) peptide (synthesized by Mimotopes), at a concentration

Table 2. **Refinement statistics used in this paper**

Variable	Value
Unique reflections[a]	30,887
R factor	18.59
R_{free}	24.36
Refined atoms	
Protein non-H atoms	5,375
Solvent	120
r.m.s. deviations	
Bond lengths (Å)	0.009
Bond angles	1.173
Ramachandran analysis	
Most favored (%)	92.8
Additionally allowed	6.5
Generously allowed	0.3
Disallowed	0.3

R_{free} is the same for the test set (5% of the data). R factor = Σ_{hkl} $||F_o| - k|F_c||/\Sigma_{hkl}$ $|F_o|$, in which k is the scaling factor, F_c is the calculated amplitude of the structure factor, and F_o is the observed amplitude of the structure factor. ESRF, European Synchrotron Radiation Facility; r.m.s., root-mean-square.
[a]This number does not include the free R set of reflections (5% of total reflections).

of 40 nM, was mixed with increasing concentrations of Bub1(1–150) in PBS buffer, and reaction mixtures were incubated at 4°C for 1 h. 5-FAM–labeled synthetic peptide Knl1(210–226) (at a concentration of 10 nM) was mixed with BubR1(1–204). Fluorescein was excited with polarized light at 485 nm, and the emitted light was detected at 535 nm through both horizontal and vertical polarizers. The K_d was determined by fitting the fluorescence polarization data to the equation $P_{obs} = P_{max}[C]/([C] + K_d)$, in which P_{obs} is the observed fluorescence polarization signal, P_{max} is the saturation value of polarization (with all the peptide in complex with the protein), and [C] is the protein concentration.

Crystallization and structure determination

Bub1(1–150) and Knl1(150–200) were mixed with molar ratio 1:1 and incubated on ice for 1 h and separated on a column (Superdex 75 10/300). The fractions containing the complex were collected, concentrated, flash frozen in liquid N_2, and stored at −80°C. The complex was set for crystallization using tris(2-carboxyethyl)phosphine as an antioxidant. Diffraction quality crystals were obtained by microseeding against 1.25 –1.3 M Na malonate, pH 6.0.

X-ray diffraction data were collected at the ID14-EH1 beamline at the European Synchrotron Radiation Facility (Grenoble, France). Data processing and reduction were performed using MOSFLM and SCALA from the CCP4 suite (Collaborative Computational Project, Number 4, 1994), and data collection statistics are provided in Table 1. Four independent monomers were placed in the asymmetric unit by molecular replacement using the program PHASER (McCoy et al., 2007) and the known Bub1 model from *S. cerevisiae* (Protein Data Bank accession no. 3ESL) as a search probe. Model optimization was performed by alternating refinement cycles with the program REFMAC (Murshudov et al., 1999) and phenix.refine from the PHENIX suite (Adams et al., 2010), and manual rebuilding was performed with COOT (Emsley et al., 2010) against a 2.6-Å dataset. The final model includes four Bub1 monomers (including residues 2–147 [chain A], 2–150 [chain B], 2–150 [chain C], and 1–148 [chain D]) and four Knl1 peptide fragments (including residues 176–187 [chain E], 176–189 [chain F], 175–189 [chain G], and 175–190 [chain H]). The parameters for the final refinement cycles can be found in Table 2. The Protein Data Bank accession no. for the atomic coordinates of the Bub1(1–150)–Knl1(150–200) complex is 4AIG.

Online supplemental material

Fig. S1 shows the expression levels of several Bub1 and BubR1 constructs discussed in this paper. Fig. S2 reports a detailed structural comparison of the complexes of the Bub1 and BubR1 TPRs with KI1 and KI2, respectively. Fig. S3 shows the localization pattern of single point mutants in the Bub1 TPR region. Fig. S4 shows additional kinase assays and loading controls for experiments in Fig. 7. Fig. S5 complements Fig. 8 and shows additional localization experiments as well as loading controls. Online supplemental material is available at http://www.jcb.org/cgi/content/full/jcb.201110013/DC1.

We thank Mitsuhiro Yanagida, Tomomi Kiyomitsu, and Stephen S. Taylor for reagents and helpful discussions, Valentina Cecatiello for help in crystallization, Fabrizio Villa for help and reagents for kinase assays, and the members of A. Musacchio's laboratory for stimulating discussions. We also thank the staff of the European Synchrotron Radiation Facility for precious help in x-ray diffraction data collection.

Work in A. Musacchio's laboratory is funded by the European Union's Seventh Framework Program European Research Council agreement KINCON and the Integrated Project MitoSys, the Italian Association for Cancer Research, the Human Frontier Science Program, and Programmi Integrati di Oncologia Strategici 7/07. S. Santaguida was supported by fellowships from the Italian Foundation for Cancer Research. V. Krenn is supported by a predoctoral fellowship from the Boehringer Ingelheim Fonds. A. Wehenkel is the recipient of the European Molecular Biology Organization and Marie Curie Intra-European Fellowships postdoctoral fellowships.

Submitted: 4 October 2011
Accepted: 18 January 2012

References

Adams, P.D., P.V. Afonine, G. Bunkóczi, V.B. Chen, I.W. Davis, N. Echols, J.J. Headd, L.-W. Hung, G.J. Kapral, R.W. Grosse-Kunstleve, et al. 2010. PHENIX: a comprehensive Python-based system for macromolecular structure solution. *Acta Crystallogr. D Biol. Crystallogr.* 66:213–221. http://dx.doi.org/10.1107/S0907444909052925

Ashkenazy, H., E. Erez, E. Martz, T. Pupko, and N. Ben-Tal. 2010. ConSurf 2010: calculating evolutionary conservation in sequence and structure of proteins and nucleic acids. *Nucleic Acids Res.* 38:W529–W533. http://dx.doi.org/10.1093/nar/gkq399

Bolanos-Garcia, V.M., and T.L. Blundell. 2011. BUB1 and BUBR1: multifaceted kinases of the cell cycle. *Trends Biochem. Sci.* 36:141–150. http://dx.doi.org/10.1016/j.tibs.2010.08.004

Bolanos-Garcia, V.M., T. Kiyomitsu, S. D'Arcy, D.Y. Chirgadze, J.G. Grossmann, D. Matak-Vinkovic, A.R. Venkitaraman, M. Yanagida, C.V. Robinson, and T.L. Blundell. 2009. The crystal structure of the N-terminal region of BUB1 provides insight into the mechanism of BUB1 recruitment to kinetochores. *Structure*. 17:105–116. http://dx.doi.org/10.1016/j.str.2008.10.015

Bolanos-Garcia, V.M., T. Lischetti, D. Matak-Vinković, E. Cota, P.J. Simpson, D.Y. Chirgadze, D.R. Spring, C.V. Robinson, J. Nilsson, and T.L. Blundell. 2011. Structure of a Blinkin-BUBR1 complex reveals an interaction crucial for kinetochore-mitotic checkpoint regulation via an unanticipated binding site. *Structure*. 19:1691–1700. http://dx.doi.org/10.1016/j.str.2011.09.017

Boyarchuk, Y., A. Salic, M. Dasso, and A. Arnaoutov. 2007. Bub1 is essential for assembly of the functional inner centromere. *J. Cell Biol.* 176:919–928. http://dx.doi.org/10.1083/jcb.200609044

Chan, G.K., S.A. Jablonski, V. Sudakin, J.C. Hittle, and T.J. Yen. 1999. Human BUBR1 is a mitotic checkpoint kinase that monitors CENP-E functions at kinetochores and binds the cyclosome/APC. *J. Cell Biol.* 146:941–954. http://dx.doi.org/10.1083/jcb.146.5.941

Cheeseman, I.M., and A. Desai. 2008. Molecular architecture of the kinetochore-microtubule interface. *Nat. Rev. Mol. Cell Biol.* 9:33–46. http://dx.doi.org/10.1038/nrm2310

Cheeseman, I.M., J.S. Chappie, E.M. Wilson-Kubalek, and A. Desai. 2006. The conserved KMN network constitutes the core microtubule-binding site of the kinetochore. *Cell*. 127:983–997. http://dx.doi.org/10.1016/j.cell.2006.09.039

Chen, R.-H. 2002. BubR1 is essential for kinetochore localization of other spindle checkpoint proteins and its phosphorylation requires Mad1. *J. Cell Biol.* 158:487–496. http://dx.doi.org/10.1083/jcb.200204048

Collaborative Computational Project, Number 4. 1994. The CCP4 suite: programs for protein crystallography. *Acta Crystallogr. D Biol. Crystallogr.* 50:760–763. http://dx.doi.org/10.1107/S0907444994003112

D'Arcy, S., O.R. Davies, T.L. Blundell, and V.M. Bolanos-Garcia. 2010. Defining the molecular basis of BubR1 kinetochore interactions and APC/C-CDC20 inhibition. *J. Biol. Chem.* 285:14764–14776. http://dx.doi.org/10.1074/jbc.M109.082016

De Antoni, A., C.G. Pearson, D. Cimini, J.C. Canman, V. Sala, L. Nezi, M. Mapelli, L. Sironi, M. Faretta, E.D. Salmon, and A. Musacchio. 2005. The Mad1/Mad2 complex as a template for Mad2 activation in the spindle assembly checkpoint. *Curr. Biol.* 15:214–225. http://dx.doi.org/10.1016/j.cub.2005.01.038

Diederichs, K., and P.A. Karplus. 1997. Improved R-factors for diffraction data analysis in macromolecular crystallography. *Nat. Struct. Biol.* 4:269–275. http://dx.doi.org/10.1038/nsb0497-269

Elowe, S. 2011. Bub1 and BubR1: at the interface between chromosome attachment and the spindle checkpoint. *Mol. Cell. Biol.* 31:3085–3093. http://dx.doi.org/10.1128/MCB.05326-11

Elowe, S., K. Dulla, A. Uldschmid, X. Li, Z. Dou, and E.A. Nigg. 2010. Uncoupling of the spindle-checkpoint and chromosome-congression functions of BubR1. *J. Cell Sci.* 123:84–94. http://dx.doi.org/10.1242/jcs.056507

Emsley, P., B. Lohkamp, W.G. Scott, and K. Cowtan. 2010. Features and development of Coot. *Acta Crystallogr. D Biol. Crystallogr.* 66:486–501. http://dx.doi.org/10.1107/S0907444910007493

Famulski, J.K., and G.K. Chan. 2007. Aurora B kinase-dependent recruitment of hZW10 and hROD to tensionless kinetochores. *Curr. Biol.* 17:2143–2149. http://dx.doi.org/10.1016/j.cub.2007.11.037

Fernius, J., and K.G. Hardwick. 2007. Bub1 kinase targets Sgo1 to ensure efficient chromosome biorientation in budding yeast mitosis. *PLoS Genet.* 3:e213. http://dx.doi.org/10.1371/journal.pgen.0030213

Gassmann, R., A. Essex, J.-S. Hu, P.S. Maddox, F. Motegi, A. Sugimoto, S.M. O'Rourke, B. Bowerman, I. McLeod, J.R. Yates III, et al. 2008. A new mechanism controlling kinetochore-microtubule interactions revealed by comparison of two dynein-targeting components: SPDL-1 and the Rod/Zwilch/Zw10 complex. *Genes Dev.* 22:2385–2399. http://dx.doi.org/10.1101/gad.1687508

Howell, B.J., B.F. McEwen, J.C. Canman, D.B. Hoffman, E.M. Farrar, C.L. Rieder, and E.D. Salmon. 2001. Cytoplasmic dynein/dynactin drives kinetochore protein transport to the spindle poles and has a role in mitotic spindle checkpoint inactivation. *J. Cell Biol.* 155:1159–1172. http://dx.doi.org/10.1083/jcb.200105093

Howell, B.J., B. Moree, E.M. Farrar, S. Stewart, G. Fang, and E.D. Salmon. 2004. Spindle checkpoint protein dynamics at kinetochores in living cells. *Curr. Biol.* 14:953–964. http://dx.doi.org/10.1016/j.cub.2004.05.053

Hoyt, M.A., L. Totis, and B.T. Roberts. 1991. *S. cerevisiae* genes required for cell cycle arrest in response to loss of microtubule function. *Cell*. 66:507–517. http://dx.doi.org/10.1016/0092-8674(81)90014-3

Johnson, V.L., M.I.F. Scott, S.V. Holt, D. Hussein, and S.S. Taylor. 2004. Bub1 is required for kinetochore localization of BubR1, Cenp-E, Cenp-F and Mad2, and chromosome congression. *J. Cell Sci.* 117:1577–1589. http://dx.doi.org/10.1242/jcs.01006

Kang, J., M. Yang, B. Li, W. Qi, C. Zhang, K.M. Shokat, D.R. Tomchick, M. Machius, and H. Yu. 2008. Structure and substrate recruitment of the human spindle checkpoint kinase Bub1. *Mol. Cell*. 32:394–405. http://dx.doi.org/10.1016/j.molcel.2008.09.017

Kawashima, S.A., Y. Yamagishi, T. Honda, K.-I. Ishiguro, and Y. Watanabe. 2010. Phosphorylation of H2A by Bub1 prevents chromosomal instability through localizing shugoshin. *Science*. 327:172–177. http://dx.doi.org/10.1126/science.1180189

Kitajima, T.S., S.A. Kawashima, and Y. Watanabe. 2004. The conserved kinetochore protein shugoshin protects centromeric cohesion during meiosis. *Nature*. 427:510–517. http://dx.doi.org/10.1038/nature02312

Kitajima, T.S., S. Hauf, M. Ohsugi, T. Yamamoto, and Y. Watanabe. 2005. Human Bub1 defines the persistent cohesion site along the mitotic chromosome by affecting Shugoshin localization. *Curr. Biol.* 15:353–359. http://dx.doi.org/10.1016/j.cub.2004.12.044

Kiyomitsu, T., C. Obuse, and M. Yanagida. 2007. Human Blinkin/AF15q14 is required for chromosome alignment and the mitotic checkpoint through direct interaction with Bub1 and BubR1. *Dev. Cell*. 13:663–676. http://dx.doi.org/10.1016/j.devcel.2007.09.005

Kiyomitsu, T., H. Murakami, and M. Yanagida. 2011. Protein interaction domain mapping of human kinetochore protein Blinkin reveals a consensus motif for binding of spindle assembly checkpoint proteins Bub1 and BubR1. *Mol. Cell. Biol.* 31:998–1011. http://dx.doi.org/10.1128/MCB.00815-10

Klebig, C., D. Korinth, and P. Meraldi. 2009. Bub1 regulates chromosome segregation in a kinetochore-independent manner. *J. Cell Biol.* 185:841–858. http://dx.doi.org/10.1083/jcb.200902128

Kolodner, R.D., D.W. Cleveland, and C.D. Putnam. 2011. Cancer. Aneuploidy drives a mutator phenotype in cancer. *Science*. 333:942–943. http://dx.doi.org/10.1126/science.1211154

Lampson, M.A., and T.M. Kapoor. 2005. The human mitotic checkpoint protein BubR1 regulates chromosome-spindle attachments. *Nat. Cell Biol.* 7:93–98. http://dx.doi.org/10.1038/ncb1208

Larsen, N.A., J. Al-Bassam, R.R. Wei, and S.C. Harrison. 2007. Structural analysis of Bub3 interactions in the mitotic spindle checkpoint. *Proc. Natl. Acad. Sci. USA*. 104:1201–1206. http://dx.doi.org/10.1073/pnas.0610358104

Li, R., and A.W. Murray. 1991. Feedback control of mitosis in budding yeast. *Cell*. 66:519–531. http://dx.doi.org/10.1016/0092-8674(81)90015-5

Liu, D., M. Vleugel, C.B. Backer, T. Hori, T. Fukagawa, I.M. Cheeseman, and M.A. Lampson. 2010. Regulated targeting of protein phosphatase 1 to the outer kinetochore by KNL1 opposes Aurora B kinase. *J. Cell Biol.* 188:809–820. http://dx.doi.org/10.1083/jcb.201001006

Logarinho, E., T. Resende, C. Torres, and H. Bousbaa. 2008. The human spindle assembly checkpoint protein Bub3 is required for the establishment of efficient kinetochore-microtubule attachments. *Mol. Biol. Cell*. 19:1798–1813. http://dx.doi.org/10.1091/mbc.E07-07-0633

Luger, K., T.J. Rechsteiner, A.J. Flaus, M.M. Waye, and T.J. Richmond. 1997. Characterization of nucleosome core particles containing histone proteins made in bacteria. *J. Mol. Biol.* 272:301–311. http://dx.doi.org/10.1006/jmbi.1997.1235

Maldonado, M., and T.M. Kapoor. 2011a. Constitutive Mad1 targeting to kinetochores uncouples checkpoint signalling from chromosome biorientation. *Nat. Cell Biol.* 13:475–482. http://dx.doi.org/10.1038/ncb2223

Maldonado, M., and T.M. Kapoor. 2011b. Moving right along: how PP1 helps clear the checkpoint. *Dev. Cell*. 20:733–734. http://dx.doi.org/10.1016/j.devcel.2011.05.017

Malureanu, L.A., K.B. Jeganathan, M. Hamada, L. Wasilewski, J. Davenport, and J.M. van Deursen. 2009. BubR1 N terminus acts as a soluble inhibitor of cyclin B degradation by APC/C(Cdc20) in interphase. *Dev. Cell*. 16:118–131. http://dx.doi.org/10.1016/j.devcel.2008.11.004

McCoy, A.J., R.W. Grosse-Kunstleve, P.D. Adams, M.D. Winn, L.C. Storoni, and R.J. Read. 2007. Phaser crystallographic software. *J. Appl. Cryst.* 40:658–674. http://dx.doi.org/10.1107/S0021889807021206

Meraldi, P., and P.K. Sorger. 2005. A dual role for Bub1 in the spindle checkpoint and chromosome congression. *EMBO J.* 24:1621–1633. http://dx.doi.org/10.1038/sj.emboj.7600641

Meraldi, P., V.M. Draviam, and P.K. Sorger. 2004. Timing and checkpoints in the regulation of mitotic progression. *Dev. Cell*. 7:45–60. http://dx.doi.org/10.1016/j.devcel.2004.06.006

Murshudov, G.N., A.A. Vagin, A. Lebedev, K.S. Wilson, and E.J. Dodson. 1999. Efficient anisotropic refinement of macromolecular structures using FFT. *Acta Crystallogr. D Biol. Crystallogr.* 55:247–255. http://dx.doi.org/10.1107/S090744499801405X

Musacchio, A., and E.D. Salmon. 2007. The spindle-assembly checkpoint in space and time. *Nat. Rev. Mol. Cell Biol.* 8:379–393. http://dx.doi.org/10.1038/nrm2163

Pagliuca, C., V.M. Draviam, E. Marco, P.K. Sorger, and P. De Wulf. 2009. Roles for the conserved spc105p/kre28p complex in kinetochore-microtubule binding and the spindle assembly checkpoint. *PLoS ONE*. 4:e7640. http://dx.doi.org/10.1371/journal.pone.0007640

Perera, D., V. Tilston, J.A. Hopwood, M. Barchi, R.P. Boot-Handford, and S.S. Taylor. 2007. Bub1 maintains centromeric cohesion by activation of the spindle checkpoint. *Dev. Cell*. 13:566–579. http://dx.doi.org/10.1016/j.devcel.2007.08.008

Petrovic, A., S. Pasqualato, P. Dube, V. Krenn, S. Santaguida, D. Cittaro, S. Monzani, L. Massimiliano, J. Keller, A. Tarricone, et al. 2010. The MIS12 complex is a protein interaction hub for outer kinetochore assembly. *J. Cell Biol.* 190:835–852. http://dx.doi.org/10.1083/jcb.201002070

Rischitor, P.E., K.M. May, and K.G. Hardwick. 2007. Bub1 is a fission yeast kinetochore scaffold protein, and is sufficient to recruit other spindle checkpoint proteins to ectopic sites on chromosomes. *PLoS ONE*. 2:e1342. http://dx.doi.org/10.1371/journal.pone.0001342

Rosenberg, J.S., F.R. Cross, and H. Funabiki. 2011. KNL1/Spc105 recruits PP1 to silence the spindle assembly checkpoint. *Curr. Biol.* 21:942–947. http://dx.doi.org/10.1016/j.cub.2011.04.011

Santaguida, S., and A. Musacchio. 2009. The life and miracles of kinetochores. *EMBO J.* 28:2511–2531. http://dx.doi.org/10.1038/emboj.2009.173

Santaguida, S., A. Tighe, A.M. D'Alise, S.S. Taylor, and A. Musacchio. 2010. Dissecting the role of MPS1 in chromosome biorientation and the spindle checkpoint through the small molecule inhibitor reversine. *J. Cell Biol.* 190:73–87. http://dx.doi.org/10.1083/jcb.201001036

Schittenhelm, R.B., R. Chaleckis, and C.F. Lehner. 2009. Intrakinetochore localization and essential functional domains of *Drosophila* Spc105. *EMBO J.* 28:2374–2386. http://dx.doi.org/10.1038/emboj.2009.188

Screpanti, E., A. De Antoni, G.M. Alushin, A. Petrovic, T. Melis, E. Nogales, and A. Musacchio. 2011. Direct binding of Cenp-C to the Mis12 complex joins the inner and outer kinetochore. *Curr. Biol.* 21:391–398. http://dx.doi.org/10.1016/j.cub.2010.12.039

Shah, J.V., E. Botvinick, Z. Bonday, F. Furnari, M. Berns, and D.W. Cleveland. 2004. Dynamics of centromere and kinetochore proteins; implications for checkpoint signaling and silencing. *Curr. Biol.* 14:942–952.

Sharp-Baker, H., and R.H. Chen. 2001. Spindle checkpoint protein Bub1 is required for kinetochore localization of Mad1, Mad2, Bub3, and CENP-E, independently of its kinase activity. *J. Cell Biol.* 153:1239–1250. http://dx.doi.org/10.1083/jcb.153.6.1239

Sironi, L., M. Melixetian, M. Faretta, E. Prosperini, K. Helin, and A. Musacchio. 2001. Mad2 binding to Mad1 and Cdc20, rather than oligomerization, is required for the spindle checkpoint. *EMBO J.* 20:6371–6382. http://dx.doi.org/10.1093/emboj/20.22.6371

Storchová, Z., J.S. Becker, N. Talarek, S. Kögelsberger, and D. Pellman. 2011. Bub1, Sgo1, and Mps1 mediate a distinct pathway for chromosome biorientation in budding yeast. *Mol. Biol. Cell*. 22:1473–1485. http://dx.doi.org/10.1091/mbc.E10-08-0673

Tang, Z., H. Shu, D. Oncel, S. Chen, and H. Yu. 2004a. Phosphorylation of Cdc20 by Bub1 provides a catalytic mechanism for APC/C inhibition by the spindle checkpoint. *Mol. Cell*. 16:387–397. http://dx.doi.org/10.1016/j.molcel.2004.09.031

Tang, Z., Y. Sun, S.E. Harley, H. Zou, and H. Yu. 2004b. Human Bub1 protects centromeric sister-chromatid cohesion through Shugoshin during mitosis. *Proc. Natl. Acad. Sci. USA*. 101:18012–18017. http://dx.doi.org/10.1073/pnas.0408600102

Taylor, S.S., and F. McKeon. 1997. Kinetochore localization of murine Bub1 is required for normal mitotic timing and checkpoint response to spindle damage. *Cell*. 89:727–735. http://dx.doi.org/10.1016/S0092-8674(00)80255-X

Taylor, S.S., E. Ha, and F. McKeon. 1998. The human homologue of Bub3 is required for kinetochore localization of Bub1 and a Mad3/Bub1-related protein kinase. *J. Cell Biol.* 142:1–11. http://dx.doi.org/10.1083/jcb.142.1.1

Taylor, S.S., D. Hussein, Y. Wang, S. Elderkin, and C.J. Morrow. 2001. Kinetochore localisation and phosphorylation of the mitotic checkpoint components Bub1 and BubR1 are differentially regulated by spindle events in human cells. *J. Cell Sci.* 114:4385–4395.

Vaur, S., F. Cubizolles, G. Plane, S. Genier, P.K. Rabitsch, J. Gregan, K. Nasmyth, V. Vanoosthuyse, K.G. Hardwick, and J.-P. Javerzat. 2005. Control of Shugoshin function during fission-yeast meiosis. *Curr. Biol.* 15:2263–2270. http://dx.doi.org/10.1016/j.cub.2005.11.034

Vigneron, S., S. Prieto, C. Bernis, J.-C. Labbé, A. Castro, and T. Lorca. 2004. Kinetochore localization of spindle checkpoint proteins: who controls whom? *Mol. Biol. Cell*. 15:4584–4596. http://dx.doi.org/10.1091/mbc.E04-01-0051

Wang, F., N.P. Ulyanova, M.S. van der Waal, D. Patnaik, S.M.A. Lens, and J.M.G. Higgins. 2011. A positive feedback loop involving Haspin and Aurora B promotes CPC accumulation at centromeres in mitosis. *Curr. Biol.* 21:1061–1069. http://dx.doi.org/10.1016/j.cub.2011.05.016

Wang, X., J.R. Babu, J.M. Harden, S.A. Jablonski, M.H. Gazi, W.L. Lingle, P.C. de Groen, T.J. Yen, and J.M. van Deursen. 2001. The mitotic checkpoint protein hBUB3 and the mRNA export factor hRAE1 interact with GLE2p-binding sequence (GLEBS)-containing proteins. *J. Biol. Chem.* 276:26559–26567. http://dx.doi.org/10.1074/jbc.M101083200

Welburn, J.P.I., M. Vleugel, D. Liu, J.R. Yates III, M.A. Lampson, T. Fukagawa, and I.M. Cheeseman. 2010. Aurora B phosphorylates spatially distinct targets to differentially regulate the kinetochore-microtubule interface. *Mol. Cell*. 38:383–392. http://dx.doi.org/10.1016/j.molcel.2010.02.034

Windecker, H., M. Langegger, S. Heinrich, and S. Hauf. 2009. Bub1 and Bub3 promote the conversion from monopolar to bipolar chromosome attachment independently of shugoshin. *EMBO Rep.* 10:1022–1028. http://dx.doi.org/10.1038/embor.2009.183

Wojcik, E., R. Basto, M. Serr, F. Scaërou, R. Karess, and T. Hays. 2001. Kinetochore dynein: its dynamics and role in the transport of the Rough deal checkpoint protein. *Nat. Cell Biol.* 3:1001–1007. http://dx.doi.org/10.1038/ncb1101-1001

Wu, J.Q., J.Y. Guo, W. Tang, C.-S. Yang, C.D. Freel, C. Chen, A.C. Nairn, and S. Kornbluth. 2009. PP1-mediated dephosphorylation of phosphoproteins at mitotic exit is controlled by inhibitor-1 and PP1 phosphorylation. *Nat. Cell Biol.* 11:644–651. http://dx.doi.org/10.1038/ncb1871

Yamagishi, Y., T. Honda, Y. Tanno, and Y. Watanabe. 2010. Two histone marks establish the inner centromere and chromosome bi-orientation. *Science*. 330:239–243. http://dx.doi.org/10.1126/science.1194498

Yamaguchi, S., A. Decottignies, and P. Nurse. 2003. Function of Cdc2p-dependent Bub1p phosphorylation and Bub1p kinase activity in the mitotic and meiotic spindle checkpoint. *EMBO J.* 22:1075–1087. http://dx.doi.org/10.1093/emboj/cdg100

Zhang, Y., and D.C. Chan. 2007. Structural basis for recruitment of mitochondrial fission complexes by Fis1. *Proc. Natl. Acad. Sci. USA*. 104:18526–18530. http://dx.doi.org/10.1073/pnas.0706441104